

THE AGES, METALLICITIES AND ALPHA ELEMENT ENHANCEMENTS OF GLOBULAR CLUSTERS IN THE ELLIPTICAL NGC 5128: A HOMOGENEOUS SPECTROSCOPIC STUDY WITH GEMINI/GMOS

KRISTIN A. WOODLEY^{1,2}, WILLIAM E. HARRIS¹, THOMAS H. PUZIA^{3,4}, MATÍAS GÓMEZ⁵, GRETCHEN L. H. HARRIS⁶, DOUG GEISLER⁷

Draft version August 27, 2018

ABSTRACT

We present new integrated light spectroscopy of globular clusters in NGC 5128, a nearby giant elliptical galaxy less than 4 Mpc away, in order to measure radial velocities and derive ages, metallicities, and alpha-element abundance ratios. Using the Gemini South 8-meter telescope with the instrument GMOS, we obtained spectroscopy in the range of $\sim 3400 - 5700 \text{ \AA}$ for 72 globular clusters with signal-to-noise greater than 30 \AA^{-1} and we have also discovered 35 new globular clusters within NGC 5128 from our radial velocity measurements. We measured and compared the Lick indices from $H\delta_A$ through Fe5406 with the single stellar population models of Thomas et al. (2003) and Thomas et al. (2004) in order to derive age, metallicity and $[\alpha/\text{Fe}]$ values. We also measure Lick indices for 41 Milky Way globular clusters from Puzia et al. (2002) and Schiavon et al. (2005) with the same methodology for direct comparison. Our results show that 68% of the NGC 5128 GCs have old ages ($> 8 \text{ Gyr}$), 14% have intermediate ages (5 – 8 Gyr), and 18% have young ages ($< 5 \text{ Gyr}$). However, when we look at the metallicity of the globular clusters as a function of age, we find 92% of metal-poor GCs and 56% of metal-rich GCs in NGC 5128 have ages $> 8 \text{ Gyr}$, indicating that the majority of both metallicity subpopulations of globular clusters formed early, with a significant population of young and metal-rich globular clusters forming later. Our metallicity distribution function generated directly from spectroscopic Lick indices is clearly bimodal, as is the color distribution of the same set of globular clusters. Thus the metallicity bimodality is real and not an artifact of the color to metallicity conversion. However, the metallicity distribution function obtained from comparison with the single stellar population models is consistent with a unimodal, bimodal, or multimodal shape. The $[\alpha/\text{Fe}]$ values are supersolar with a mean value of 0.14 ± 0.04 , indicating a fast formation timescale. However, the GCs in NGC 5128 are not as $[\alpha/\text{Fe}]$ enhanced as the Milky Way GCs also examined in this study. Our measured indices also indicate that the globular clusters in NGC 5128 may have a slight overabundance in nitrogen and a wider range of calcium strength compared to the Milky Way globular clusters. Our results support a rapid, early formation of the globular cluster system in NGC 5128, with subsequent major accretion and/or GC and star forming events in more recent times.

Subject headings: galaxies: elliptical and lenticular, cD — galaxies: evolution — galaxies: individual (NGC 5128) galaxies: star clusters — globular clusters: general

1. INTRODUCTION

The star formation history of early-type galaxies is quite complex with evidence supporting episodes of star formation at both high and low redshifts. At high redshifts ($z > 2$), the formation of the bulk of the galactic stellar component is supported by, for example, the fundamental plane relation (Djorgovski & Davis 1987; Dressler et al. 1987; Treu et al. 1999) in the monolithic collapse scenario (Eggen et al. 1962; Tinsley 1972; Larson 1974, 1975; Silk 1977; Arimoto & Yoshii 1987). The hierarchical merging scenario (Toomre 1977; White & Rees

1978; Peebles 1980; White & Frenk 1991; Kauffmann et al. 1993; Baugh et al. 1998; Cole et al. 2000; Somerville et al. 2001) on the other hand, predicts a range of formation timescales for the stellar component down to much lower redshift values. In the extreme case, gas-rich merging galaxies are seen today where young star clusters, for example in NGC 4038/4039 (Whitmore & Schweizer 1995), and/or young and intermediate aged globular clusters (GCs) have been detected, indicating that GCs, as well as a fraction of the stellar component of the galaxy can form at $z \leq 1$.

The key to understanding the formation epochs of these types of galaxies is through their star formation history. Most early-type galaxies are too distant to resolve stars from which we can measure their ages directly. Unresolved light studies are difficult as well, as they are hindered by the age-metallicity degeneracy (Mould & Aaronson 1980, and references therein) as well as internal extinction in the galaxies.

GCs, on the other hand, are essentially coeval structures that form with nearly single age and single metallicity. They have been used, therefore, as powerful tools to trace the complex star formation history of early-type

¹ Department of Physics & Astronomy, McMaster University, Hamilton ON L8S 4M1, Canada; harris@physics.mcmaster.ca

² Current Address: Department of Physics & Astronomy, University of British Columbia, Vancouver, BC V6T 1Z1, Canada; kwoodley@phas.ubc.ca

³ Herzberg Institute of Astrophysics, 5071 West Saanich Road, Victoria, BC V9E 2E7, Canada; thomas.puzia@nrc.ca

⁴ Plaskett Fellow

⁵ Departamento de Ciencias Físicas, Facultad de Ingeniería, Universidad Andres Bello, Chile; matiasgomez@unab.cl

⁶ Department of Physics and Astronomy, University of Waterloo, Waterloo, ON N2L 3G1, Canada; gharris@astro.uwaterloo.ca

⁷ Departamento de Astronomía, Universidad de Concepción, Chile; dgeisler@astro-udec.cl

galaxies. Their internal properties, such as ages and metallicities are used as representations of the overall stellar component of the galaxy. We also benefit from the use of GCs as they do not suffer from problems involving internal reddening. GCs can be used as good tracers of the time period of early-type galaxy formation because we can determine their ages, metallicities, and alpha-enhancements through their spectra. By examining the ratio of GCs that are old to GCs with younger ages, as well as comparing the age difference between metal-rich and metal-poor GCs, we can determine which formation scenario is dominant.

Previous studies using photometry to determine ages and metallicities of GCs are plagued with age-metallicity degeneracies, especially in the optical regime (Worthey 1994). One way to avoid the age-metallicity degeneracy using photometry is through the use of (near-)infrared data, which is mainly sensitive to the metallicity of the red giant branch, combined with optical data, sensitive to both age and metallicity. This technique has been shown to be effective at distinguishing between GC populations that appear to be single-aged and old such as NGC 7192 (Hempel et al. 2003), NGC 1399 (Kundu et al. 2005), and NGC 3115 (Puzia et al. 2002), versus those with a wide spread of ages such as NGC 4365 (Puzia et al. 2002; Kundu et al. 2005) and NGC 5846 (Hempel et al. 2003, 2007). However, a sample of GCs in NGC 4365 with intermediate ages were found to have old ages using spectroscopic techniques (Brodie et al. 2005). These color indices are also not precise enough to be useful for individual GCs or to derive genuine age distribution functions.

Spectroscopy allows us to determine the internal properties of individual GCs as long as we have high signal-to-noise data. The measurement of the strength of absorption line features in the spectra enables us to obtain ages, metallicities, and $[\alpha/\text{Fe}]$ through comparison with SSP models. This technique enables the collection of a significant fraction of both metal-rich and metal-poor GC data in one environment that can show the formation epoch(s) and chemical composition at the time of formation of the GCs within one early-type galaxy.

The proximity of NGC 5128 makes this early-type galaxy extremely attractive to conduct a large, homogeneous age and metallicity study (3.8 ± 0.1 Mpc Harris et al. 2009). Features within this galaxy (the dust lane and faint shells (Malin 1978), visible star formation from the interaction of the radio jet with the shells of HI (Graham 1998), and a young tidal stream in the halo (Peng et al. 2002)) are recent phenomena which will have little bearing on the much older GC population.

Previous studies have been able to obtain spectroscopy for GCs in many different galaxies to determine global properties of the metal-poor versus metal-rich clusters (Puzia et al. 2005a; Strader et al. 2005; Sharina et al. 2006, among others). Within NGC 5128, we should be able to determine whether there is a significant fraction of young or intermediate-aged GCs, or if the majority are old, similar to their Milky Way GC counterparts. Our primary goal is to use a large and high signal-to-noise (S/N) sample of GC spectra within NGC 5128 to obtain the relative age difference between the metal-rich and the metal-poor clusters. Currently, we have the advantage of knowing over 415 GCs in NGC 5128 which have

been confirmed with either radial velocity measurement and/or HST images cataloged in Woodley et al. (2007). This catalog has provided the database from which we selected our target objects.

We present our results in the sections below: section 2 describes our data set and its reduction; section 3 describes the radial velocity measurements obtained and the confirmation of newly discovered GCs; section 4 describes the calibration of our data and our resulting ages, metallicities, and $[\alpha/\text{Fe}]$; section 5 discusses our findings; and we conclude in Section 6.

2. DATA SAMPLE AND REDUCTION TECHNIQUES

2.1. Gemini/GMOS Dataset

We obtained low-resolution spectroscopy of known and candidate GCs with the Gemini South 8-meter telescope using the Gemini Multi-Object Spectrograph (GMOS). We placed 8 fields around the center of NGC 5128, covering the inner 15 kpc of the halo over two observing periods, program IDs GS-2005A-Q-28 (PI: William E. Harris) and GS-2007A-Q-55 (PI: Doug Geisler). The GMOS instrument allows us to obtain spectroscopy of multiple objects in each 5.5' field of view. The 8 masks each contained between 18 and 25 objects observed through 0.5'' slits, totalling 176 objects (see Table 1). Typical exposures were taken in multiples of 1800 second intervals, totalling 3 – 3.75 hours per field. The central wavelengths were split among 447 nm, 450 nm, and 453 nm in order to interpolate across the chip gaps between the CCDs. The mean wavelength coverage of the data is $\sim 3400 - 5700\text{\AA}$, safely including the major absorption features, in the blue region of the spectra from Ca H+K to redward of Mgb, for the majority of our target objects. All exposures used no filter and the grating B600+G5232 with a blaze wavelength of 461 nm. The 2005 data were binned 4 times in the spectral and 2 times in the spatial direction and a spectral resolution of $1.8\text{\AA}/\text{px}$. The 2007 data were binned 2 times in the spectral and unbinned in the spatial directions and a spectral resolution of $0.9\text{\AA}/\text{px}$. A gain of $2.07\text{ e}^-/\text{ADU}$ and a readout noise of 3.69 e^- for all data were chosen.

Each science exposure was bracketed by flat field exposures and a CuAr calibration arc with the same configuration and central wavelength. However, the 2005 data had arcs taken only at 450 nm, so we shifted the arcs using the 5577\AA night-sky emission line to calibrate the 447 and 453 nm exposures. The biases were downloaded from the Canadian Astronomy Data Centre in the Gemini archive and were taken within the same month as each science exposure.

2.2. Data Reduction

The data reduction was completed with the Gemini package in IRAF⁸. Initially, the data were prepared with the task *gprepare* followed by the bias and trimming of the science fields and flat fields as well as overscanning and trimming the calibration arcs (*gsreduce*). The 3 CCD chips of the calibration arcs were mosaiced (*gmosaic*) and the slits were individually cut (*gscut*). The calibration

⁸ IRAF is distributed by the National Optical Astronomy Observatories, which is operated by the Association of Universities for Research in Astronomy, Inc., under cooperative agreement with the National Science Foundation

arcs were then used to calibrate the data from pixel-to-wavelength using known spectral features (*gs wavelength*) and the flat fields were prepared by fitting the response functions of the detectors in each CCD chip (*gs flat*). A bad pixel mask was created for each CCD chip which replaced the dead pixels and the hot pixels found in the flat fields and bias frames, respectively (*im replace*). The masks were then used to replace the bad pixels in the science and flat fields (*fix pix*). The task *gs reduce* was used again to flat field, interpolate over the gaps, and mosaic the 3 CCD chips in the science spectra. A task called *mosproc*, written by Bryan W. Miller, and explained in detail in Tranco et al. (2007) was then used to perform the remaining tasks. The cosmic ray subtraction in *mosproc* was done with the van Dokkum (2001) Laplacian edge detection algorithm. The task *gs transform* was then used to rectify and apply the calibration to each spectra which were then traced, background sky subtracted, and then extracted into one-dimensional spectra with *gs extract*. Lastly, a quantum efficiency correction was applied to the data (*gecorr*).

Following the pre-reduction described above, on every exposure we isolated the segments containing each Lick-index feature and surrounding continuum. We used 20 Lick features from H δ _A to Fe5406. Each index was then cross-correlated using *fxcor* in the IRAF package *rv* with a template spectrum of a globular cluster in M31, 158-213 (Puzia et al. 2002), which was shifted to a velocity of 0 km s⁻¹. This yielded a measured radial velocity for each of the 20 features in each exposure (to be discussed in greater detail in Section 3). We then flux calibrated each individual science spectrum using standard stars taken for our observations and obtained from the CADC. Our standard stars were EG21 for the 2005 data and LTT4364 for the 2007 data. The sensitivity file as a function of wavelength was generated for the standard stars (*gs standard*) and applied to the science spectra with *calibrate* which also corrected for extinction. Following the flux calibration, each individual exposure was then shifted to 0 km s⁻¹ (*dopcor*) and then sum combined appropriately (*scombine*) for each GC.

3. RADIAL VELOCITY MEASUREMENTS AND NEWLY CONFIRMED GLOBULAR CLUSTERS

We used any spare space on our masks not occupied by a known GC in NGC 5128 to search for previously unidentified clusters. Our candidate GCs were selected from color, magnitude, and point spread function subtraction from Gemini pre-images for the 2005 dataset (*i* filter) and from 1.2 × 1.2 deg² Magellan/Inamori Magellan Areal Camera and Spectrograph (IMACS) images (*R* filter) taken in 0.5'' seeing (Harris et al. 2009, in preparation, and described briefly in Gómez & Woodley 2007) for the 2007 dataset. At the low galactic latitude of NGC 5128 ($b = 19^\circ$), we expect contamination from both background galaxies and foreground stars in the Milky Way that can have colors and magnitudes expected for normal GCs, but a powerful way to securely classify candidate objects as GCs is through radial velocity measurements. It has been shown in previous spectroscopic studies that GCs in NGC 5128, have typical $v_r = 200 - 1000$ km s⁻¹ and are thus distinguishable from foreground stars, $v_r \lesssim 200$ km s⁻¹ and background galaxies, $v_r > 1000$ km s⁻¹ (see Peng et al. 2004b; Woodley et al. 2005; Beasley

et al. 2008, for examples) at a very high level of confidence.

We obtained spectra for 101 known GCs (13 of which were measured twice) and 60 new candidate GCs. Of our candidates, 35 satisfied the velocity criterion of $v_r = 200 - 1000$ km s⁻¹ with two of these clusters measured twice. Of the remaining candidates, we ended up with 18 stars, 5 background galaxies, and 2 objects for which we were unable to obtain any correlation with our template GC. It is important to note the difference in confirmation of candidates as genuine GCs from the 2005 and 2007 observations. The typical selection of GCs from GMOS pre-images with 1'' seeing yielded a 56% hit rate of confirmed GCs. In 2007, we used high quality IMACS images for candidate selection. With the higher spatial resolution of these images, taken in excellent seeing (0.5''), we achieved an 85% hit rate.

The S/N of the GC data, measured between 4700Å – 4830Å, ranged from $\sim 10 - 200 \text{Å}^{-1}$, with a mean and median of 56Å^{-1} and 44Å^{-1} for the 2005 data and 34Å^{-1} and 32Å^{-1} for the 2007 data, respectively. Tables 2 & 3 list the results for the previously known GCs and the 35 newly confirmed GCs. The tables list the cataloged name of the GC, the old literature name of the GCs (for previously known GCs), the *R.A.* and *Decl.* in the J2000 epoch, the mask/field number and slit number (designated by m and s, respectively), the approximate S/N per Å measured around 4765 Å, and the radial velocity obtained from our cross-correlation technique. For Table 2, the final column is the weighted mean of all previously published radial velocity measurements for that GC *including* the radial velocity determined in this study. The remaining columns in Table 3 are the C, M, and T₁ Washington photometry with associated uncertainties from Harris et al. (2004).

Figure 2 shows the radial velocity distribution of our known and newly confirmed GCs. The duplicate velocities obtained for the GCs follow a 1:1 correlation quite closely with an rms error ± 32 km s⁻¹ from the least squares fit. This tight correlation indicates a strong reproducibility in our radial velocity measurements. The velocities that we obtained for the previously measured GCs matched well with those in the literature, except for three cases. GC0049 (Peng et al. 2004b), GC0188, and GC0226 (both from Beasley et al. 2008) (see the bottom panel of Fig. 2) have had only one previous radial velocity measurement and the latter two cases had high radial velocity uncertainties. All the measurements are still consistent with being genuine GCs. There appears to be a potential scale difference between our measured velocities and the cataloged velocities. For the GCs in common, there is an average radial velocity uncertainty of 34 km s⁻¹ in our study and 39 km s⁻¹ in the catalog. We have not been able to find any reason for this difference, however, the offset or scale error between the two datasets is not significant within the these measurement uncertainties.

Of our candidate objects, 4 had velocities between 150 – 250 km s⁻¹ indicating these objects may either be GCs or Milky Way foreground stars. With the quality of most spectra obtained for radial velocity studies, it is not a simple task to distinguish between these two types of objects. We decided to measure the structural

parameters of these 4 objects using our IMACS images of NGC 5128 in combination with our velocity and photometry information to help distinguish between either foreground stars or GCs. To do this, we used the code ISHAPE (Larsen 1999, 2001) which convolves the stellar point spread function with an analytical King profile (King 1962) and compares the result with the input candidate image achieving a best match. The structural parameters measured from the models are the core radius, r_c , the tidal radius, r_t , the concentration parameter, $c = r_t/r_c$, and ellipticity. The half-light radii can also be obtained from the transformation, $r_e/r_c \simeq 0.547c^{0.486}$ which is good to $\pm 2\%$ for $c > 4$ (Larsen 2001), which is satisfied for GCs in NGC 5128 (see Gómez & Woodley 2007). Based on their structural parameter values compared to normal GCs in NGC 5128 (Gómez & Woodley 2007) (as well as their velocities and photometry) we classify 3 of the 4 candidates as GCs (GC0463, GC0467, and GC0471).

The luminosity function of our newly confirmed GCs is shown in Figure 3, along with the entire GCS and the GCs with ages, metallicities, and $[\alpha/\text{Fe}]$ obtained in this study. On average, our newly confirmed GCs are fainter than the globular cluster system (GCS) turnover magnitude. This is not surprising as our long GMOS exposures permitted us to get good radial velocity measurements on fainter objects. Our targetted GCs for measurement of age, metallicity, and $[\alpha/\text{Fe}]$ were brighter than the average cluster in the system. This is also expected as we targetted the brightest GCs to meet the high S/N requirement of this study.

4. RESULTS

4.1. The Lick Index System

The standardized Lick index system (Burstein et al. 1984; Worthey et al. 1994; Worthey & Ottaviani 1997; Trager et al. 1998) provides a framework of recipes to measure the strength of absorption line features in low-resolution spectra. These calibrated Lick index measurements can be compared to SSP models in order to estimate their ages, metallicities, and $[\alpha/\text{Fe}]$.

The Lick indices were measured using the code called GONZO described in full in Puzia et al. (2002). This code measures the line index of each Lick feature according to the observer's definition of equivalent width (Worthey et al. 1994). This measures the difference between the flux of the feature compared to its pseudo-continuum. For this study, we have used the pass-band and pseudo-continuum definitions of Worthey et al. (1994) and Worthey & Ottaviani (1997). The input spectra and variance spectra are used within GONZO to generate the uncertainty of the Lick index measurements through the addition of Poisson noise via 100 Monte-Carlo simulations. The indices are measured on the noise enhanced spectra and the 1σ standard deviation of the measured index is the total Lick index uncertainty.

The calibrated indices and their bootstrapped uncertainties are listed in Tables 4 & 5, respectively. For GCs that were measured more than once, only the indices for the highest-S/N spectra and/or the spectra which had the most measureable indices are listed. For some red indices there is no recorded measurement due to the placement of the GC on the mask. For most of these

latter objects, it is was therefore not possible to obtain ages, metallicities and $[\alpha/\text{Fe}]$ from the SSP models.

4.2. Data Calibration to the Lick System

Our GMOS data were calibrated onto the Lick system with a secondary standard star method. Beasley et al. (2008) have obtained spectroscopy of GCs in NGC 5128 using the Anglo Australian Telescope (AAT) + 2dF and have calibrated their measured indices to the standard Lick index system with 12 Lick standard stars. We have a number of GCs in common with Beasley et al. (2008) from both our 2005 and 2007 GMOS data sets. We show the comparison of the indices in Figure 4 for the 2005 data and Figure 5 for the 2007 data. The number of calibrating GCs in common (once deviants $> 2\sigma$ have been removed) ranged from 14 – 22 with an average of ~ 18 for the 2005 data and 9 – 16 with an average of ~ 14 for the 2007 data. From Figs. 4 & 5, it is clear that a simple zeropoint shift is a valid correction of our system to the standard Lick system. The mean shift between the AAT and GMOS data sets was then applied to the GMOS data in order to calibrate it to the Lick system. Our typical shifts were 0.41\AA and 0.10 mag.

We also took integrated light spectroscopy for 40 Milky Way GCs (excluding NGC 6254 from the 41 available spectra) from Schiavon et al. (2005) available online. We measured their absorption features and calibrated them to the Lick system using 11 GCs in common with Puzia et al. (2002). We added one additional GC, NGC 6981, from Puzia et al. (2002) that was not included in Schiavon et al. (2005). The comparisons of the Lick indices and the adopted shifts are shown in Figure 6. The indices Fe4383 and Fe5015 were not used in these results because the spectroscopy from Schiavon et al. (2005) had defects from the CCD or poor sky subtraction in the regions of these two features. We obtained ages, metallicities, and $[\alpha/\text{Fe}]$ of the Milky Way GCs with the same methodology as we did for GCs in NGC 5128. In this way, we permit the most direct possible comparison between the two galaxies.

4.3. The Measured Lick Indices

In Figure 7 we show the measured indices of the GCs in NGC 5128 and the Milky Way for $\text{H}\beta$, $\text{H}\delta_A$, $\text{H}\delta_F$, $\text{H}\gamma_A$, and $\text{H}\gamma_F$ versus $[\text{MgFe}]'$. $[\text{MgFe}]'$ is a composite index that has been shown to be insensitive to varying $[\alpha/\text{Fe}]$. It is defined as $[\text{MgFe}]' = \sqrt{\text{Mg}_b} \times (0.72 \times \text{Fe}5270 + 0.28 \times \text{Fe}5335)$ (Thomas et al. 2003). Overplotted are the SSP models of Thomas et al. (2003) and Thomas et al. (2004) for the grids of $[\alpha/\text{Fe}] = 0$.

We see the majority of GCs for both systems lie off the model grids with extremely old ages that would be inconsistent with the WMAP age of the Universe (Spergel et al. 2003). This is a general problem for all studies of integrated light GC spectroscopy applied to the presently available model grids. The internal uncertainties for indices from high-S/N spectroscopy are very low, as seen in Fig. 7, and these measured uncertainties will not get much lower for extragalactic GCs because $\text{S/N} > 100$ is hard to achieve. However, we still find that they generally do not match the model grids of SSPs. The SSP models are calibrated on the integrated-light optical pho-

tometry of Milky Way GCs and high-resolution spectroscopy of individual member stars. There must be further astrophysics, therefore, that needs to be incorporated into these models in order to directly match the indices of GCs.

Also shown in Fig. 7 are the plotted indices of $\langle \text{Fe} \rangle = (\text{Fe}5270 + \text{Fe}5335)/2$ and Mg_2 , which allow a clear separation of the 3 different model $[\alpha/\text{Fe}]$ grid lines of 0, 0.3, and 0.5. The majority of GCs in NGC 5128 fall between $[\alpha/\text{Fe}] = 0 - 0.3$, as do the Milky Way GCs.

We can also look at the diagnostic plots of indices that provide information on the abundances of calcium, carbon, and nitrogen (Tripicco & Bell 1995) in Figure 8. The strength of the calcium index is shown in the diagnostic plot of Ca4227. There is a large amount of scatter, both overabundant and underabundant for the GCs in NGC 5128, unlike the Milky Way GCs which follow the SSP model grids quite closely. However, the calibrations of Ca4227 to the Lick index system, shown in Figs. 4 & 5, have a large scatter which could artificially produce the calcium scatter seen in Fig. 8. Looking at the plot of CN_2 , we see clear indications for systematically stronger index strengths (i.e. a carbon/nitrogen overabundance) for the GCs in NGC 5128 and some GCs in the Milky Way with respect to the model grids. This cannot be accounted for solely by variations in $[\alpha/\text{Fe}]$ or by age-metallicity degeneracy of the grids. Rather this indicates an overabundance in carbon and/or nitrogen.

The index strengths of G4300 and C_24668 have been shown to have sensitivity to carbon abundance but only weak sensitivity to the nitrogen abundance (Tripicco & Bell 1995). In Fig. 8, we see a mild overabundance in G4300, but not in C_24668 . The C_24668 index appears to have a small scatter centered on the model grids. This indicates that the GCs in NGC 5128 may have a slight overabundance in nitrogen and a wider range of calcium index strength compared to the Milky Way GCs. The implication of this result, however, is unclear. Puzia & Sharina (2008) found evidence for a varying nitrogen abundance with little evidence for a carbon enhancement in their recent study of GCs in low surface brightness dwarf galaxies. Our abundance trends for these elements do, however, agree with the general results of GCs in M31 (Puzia et al. 2005b), which as a giant galaxy of comparable luminosity to NGC 5128 is likely to be a closer analog than the dwarfs. More evidence is needed to understand if the abundance trends found in GCs have environmental dependences.

The ages, metallicities, and $[\alpha/\text{Fe}]$ were determined by iterating between the measured indices and the SSP models of Thomas et al. (2003) and Thomas et al. (2004) (described in Puzia 2003; Puzia et al. 2005a). The indices used in the iteration process are the Balmer lines, Mg_2 , Mg_b , Fe5270, and Fe5335. For the GCs that fall outside of the model grids, a value of 15 Gyr in age is assumed. Typically these GCs have a higher uncertainty in their measured index and thus a lower weighting in the final generated age value attributed to the GC. The measurement routine iterates between the diagnostic plots of indices and once convergence is reached it provides an age, a metallicity and an $[\alpha/\text{Fe}]$ estimate and their uncertainties for each input GC (see Table 6). With our Lick index measurement routines, we are able to obtain low internal statistical uncertainties on the ages ($\Delta t/t \sim 0.3$),

metallicities ($\Delta Z \sim 0.15$ dex), and $[\alpha/\text{Fe}]$ ($\Delta[\alpha/\text{Fe}] \sim 0.1$ dex) crucial for constraining different formation scenarios from a differential analysis. There were 4 GCs in NGC 5128 that had ages, metallicities, and $[\alpha/\text{Fe}]$ measured from two different spectra obtained in this study. The root mean square of the 4 multiple measurements are ± 2.4 Gyr for age, ± 0.2 dex for metallicity, and ± 0.5 dex for $[\alpha/\text{Fe}]$ (see Table 6 for the multiple measurements).

The ages for the Milky Way GCs determined in this study can be directly compared to relative ages recently derived by Marín-Franch et al. (2008), obtained from main sequence fitting on HST/ACS color magnitude diagrams of 64 Milky Way GCs. This comparison provides an excellent external validation on the Lick index ages that we derive for the NGC 5128 GCs. The comparison of the 24 overlapping Milky Way GCs with this study is shown in Figure 9. Clearly, the two techniques do not produce a precise 1:1 correlation in their results, however the ages derived by both studies are consistently old. The scatter shows the Lick index routine underestimates the ages of the Milky Way GCs by about 1 Gyr for the younger GCs, while it overestimates the ages for the oldest GCs. This could lead to an artificial spread in our determined ages for the GCs in NGC 5128 and may overestimate the number of young GCs. We note that the horizontal spread in data is about twice as large as the vertical spread, indicating that the internal scatter of the main sequence fitting routine is about 1/2 of the Lick system method.

4.4. Ages of the GCs in NGC 5128

Figure 10 shows the age, metallicity, and $[\alpha/\text{Fe}]$ distributions for 72 individual GCs in NGC 5128 with $\text{S/N} > 30 \text{ \AA}^{-1}$ and for 41 Milky Way GCs. The histograms have been fit with Gaussian distributions using the statistical code RMIX⁹, a library written with the statistics programming language, R. RMIX allows a range of multimodal fitting, including the functional form of the curve, and hetero- and homo-scedastic fitting cases. The histograms have been fit with unimodal, bimodal, and trimodal Gaussian distributions, with the fitted values as well as reduced χ^2 listed in Table 7. We have also included in Table 7 the probability, listed as the p-value, that the data are drawn from this distribution. When there is no result listed in the table, we were unable to obtain a fit using RMIX. The fits with the lowest reduced χ^2 are shown as solid lines in Fig. 10 along with its reduced χ^2 value. For the GCs in NGC 5128 we were able to obtain additional bimodal and/or trimodal fits with nearly equal reduced χ^2 values for $[\text{Z}/\text{H}]$ and $[\alpha/\text{Fe}]$ indicating that they are also fit well by these alternate modalities.

The age estimates provided by the iterative code enable us to distinguish among old (> 8 Gyr), intermediate ($5 - 8$ Gyr), and young (< 5 Gyr, forming at $z \leq 1.2$) stellar populations within our uncertainties. The Gaussian fits to the NGC 5128 data suggest two or three major bursts of cluster formation within this galaxy and a rejection of the single burst solution. More specifically,

⁹ The complete code, available for a variety of platforms, is publicly available from Peter MacDonald's Web site at <http://www.math.mcmaster.ca/peter/mix/mix.html>. The same site gives links to an extensive bibliography with further examples of its use.

68% of our sample have old ages, 14% have intermediate ages, and 18% have young ages. For the Milky Way GCs, interestingly, the best statistical fit is a bimodal distribution, with both peaks at nearly the same formation time in agreement with the results of Marín-Franch et al. (2008). A Kolmogorov-Smirnov statistical comparison test indicates the normalized age distributions of NGC 5128 and Milky Way GCs are different at greater than a 99% confidence level.

Also in Fig. 10 is the histogram of all 64 Milky Way GCs obtained by Marín-Franch et al. (2008). Their results are ~ 1 Gyr older on average than our ages obtained using the Lick index method (see Fig. 9). Our spectroscopic Lick index study also shows a small extension to younger ages for the Milky Way clusters, not seen in Marín-Franch et al. (2008). However, out of the 6 Milky Way GCs for which we have measured ages < 10 Gyr, only 3 of these were measured by Marín-Franch et al. (2008).

In contrast to NGC 5128, it appears nearly all GCs in the Milky Way have formed primordially, with a small fraction of younger GCs, perhaps obtained from the accretion of satellite galaxies. We do detect a positive age-metallicity slope relation in the Milky Way clusters, also noted by Mendel et al. (2007). The 41 Milky Way GCs have a mean of 11.3 ± 0.1 Gyr and only one GC (NGC 6553) has a determined age less than 8 Gyr. This particular result could be illustrating one of the generic problems with using SSP models to derive internal properties of GCs from integrated light spectroscopy. NGC 6553 has been shown to be an old GC (Ortolani et al. 1995) and one of the most metal-rich (Barbuy et al. 1998) in the Milky Way. Our results do provide a metal-rich $[Z/H]$ value of 0.14 ± 0.01 , but it is the youngest of our sample (6.7 ± 0.2 Gyr). The result indicates once again that this methodology could be underestimating the ages of the metal-rich GCs. This could, in part, be attributed to horizontal branch stars and blue stragglers that have been shown to mimic a younger stellar population (Burstein et al. 1984; Cennaro et al. 2009). These hot stellar populations are incorporated into SSP models, however are still based on individual star spectroscopy within Milky Way GCs, whereas here, we are using integrated spectroscopy. However, NGC 6553 is projected onto the bulge stellar population of the Milky Way as it sits in Baade’s Window. In this region, a good background subtraction is crucial as to not artificially enhance the measured Lick indices, particularly the Balmer lines. Alternatively, or perhaps in conjunction with, NGC 6553 has a high blue straggler specific frequency with evidence for spatial variation (see Figure 12 of Beaulieu et al. 2001). NGC 6553 also has an anomalously blue horizontal branch for its high metallicity that could influence the Lick measurements depending on where the study focused in the GC itself, leading to a over or undersampling of the true GC blue straggler contribution.

4.5. Metallicities of the GCs in NGC 5128

The GCs in NGC 5128 used in this study were biased towards more enriched metallicities based on our selected field location concentrated towards the inner $10'$. We find over 65% of GCs have $[Z/H] > -1$, while larger samples of GCs in NGC 5128 show a near 50-50% split between the metal-rich and metal-poor cluster popula-

tion (see Woodley et al. 2005, for example). This stems from the metallicity gradient where the metal-rich GCs are more centrally concentrated than the metal-poor (see Woodley et al. 2005, 2007; Beasley et al. 2008). This bias leads to an artificial inflation of young, metal-rich GCs relative to the entire halo. In addition, we would expect the inner few arcmins of the galaxy to show the largest range of ages and formation timescales because accreted material will sink to the central regions of the galaxy.

We compare the different Gaussian distributions of color and metallicity obtained from this study in Figure 11 using our sample of 68 GCs in NGC 5128 that have both metallicity obtained from the SSP models as well as available color information. The color distribution, $(C-T_1)$ (Harris et al. 2004), and the metallicity, $[Fe/H]_{C-T_1}$, obtained from a color transformation, are plotted. This transformation of color-to-metallicity has been calibrated through Milky Way GC data (Harris & Harris 2002). We use a foreground reddening value of $E(B - V) = 0.11$ for NGC 5128, corresponding to $E(C - T_1) = 0.22$ for the transformation. This transformation is slightly nonlinear so the uncertainty in $[Fe/H]$ is a function of metallicity. The uncertainties for a typical color uncertainty of 0.1 are ± 0.07 dex in the metal-rich and ± 0.2 dex in the metal-poor regimes. Both distributions are clearly bimodal.

We also plot the synthetic $[MgFe]'$ index for the same set of GCs, which is an almost pure metallicity indicator, shown to be weakly sensitive to age and insensitive to $[\alpha/Fe]$ (Thomas et al. 2003). The $[MgFe]'$ index is measured directly from our spectroscopy and thus, model independent. The $[MgFe]'$ distribution is adequately fit by a bimodal model, as are the Milky Way GCs, also plotted in Fig. 11. We also fit the $[MgFe]'$ index for the NGC 5128 GCs with a unimodal distribution and obtain a reduced χ^2 value of 1.02, which is significantly different than the bimodal fit. The metallicity distribution obtained from the SSP models, $[Z/H]$, shown in Fig. 10, for the clusters in NGC 5128 is consistent with a bimodal distribution, but it is not strongly preferred over other possible distributions. Yet, with the shape of the metallicity index $[MgFe]'$ distribution, we can state that both the metallicity (obtained directly from high-S/N spectroscopy) and the color distributions for the same sample of GCs, both appear bimodal. Yoon et al. (2006) have shown that a bimodal metallicity distribution can be an artifact of the non-linearity in the transformation from metallicity to color (see also Cantiello & Blakeslee 2007). We show here that the GCs in NGC 5128 have a bimodal color *and* a bimodal $[MgFe]'$ index, which is independent of any transformation between color and metallicity. This finding is further supported by the recent observations of Spitler et al. (2008) who show strong evidence for color bimodality in NGC 5128 GCs from R band to mid-IR band observations, which are insensitive to hot horizontal branch stars, and thus a good indicator of metallicity as well.

We calculate the iron abundance for the GCs in NGC 5128 obtained from the SSP models (see equation 4 in Thomas et al. 2003) and compare to that obtained from the color conversion discussed above, $[Fe/H]_{C-T_1}$ for the GCs in NGC 5128, shown in Figure 12. We perform a best linear fit which has an rms of 0.36 (after removal of deviant points based on the Chauvenet Criteria (Par-

ratt 1961)). The correlation does not match a 1:1 relationship as expected for direct comparison between the two values. It appears either $[\text{Fe}/\text{H}]$ determined from the models is too metal-rich, or the $[\text{Fe}/\text{H}]_{C-T_1}$ values obtained from the color conversion are too metal-poor. This could be the result of the small non-linearity in the color-to-metallicity conversion or a progressive change in alpha abundance with metallicity.

In Figure 13, we show $[\text{Z}/\text{H}]$ as a function of age. The majority of GCs in NGC 5128 and the Milky Way share the same relative ages in our study, but NGC 5128 contains a number of intermediate-age and young GCs. The spread in age that we find for NGC 5128 GCs is almost purely from the metal-rich subpopulation. We find, specifically, that 92% (23/25) of metal-poor GCs and 56% (26/47) of metal-rich GCs in NGC 5128 have ages > 8 Gyr. We may see evidence for an age-metallicity relation, however, no strong conclusions can be drawn from our results because of the large biases in our selected GC sample.

Massive elliptical galaxies, including NGC 5128, show a super metal-rich peak observed in the $[\text{Z}/\text{H}]$ distribution of GCs. This metal-rich peak has been predicted by the spatially resolved chemical evolution code of elliptical galaxies (Pipino & Matteucci 2004; Pipino et al. 2007) and closely matched the spectroscopically determined metal-rich $[\text{Z}/\text{H}]$ distribution of a representative sample of elliptical galaxies (Puzia et al. 2006). Their models indicate that this super metal-rich GC peak found in massive elliptical galaxies could be the result of a parent galaxy that has radially varying photochemical properties resulting from the outside-in formation mechanism (Pipino & Matteucci 2004; Pipino et al. 2006). In addition to the radially varying metallicity of the galaxy (and of the GCS), the massive elliptical would have undergone a violent merger history.

The photometric metallicity for the stellar halo for NGC 5128 is also shown in Fig. 11 for an inner region at 8 kpc and a combined outer halo field of 21 and 31 kpc, at a maximum extent of $\sim 7R_{\text{eff}}$ of the galaxy (Harris & Harris 2000, 2002; Rejkuba et al. 2005). What is strikingly evident is that the stellar halo and GC populations have very different metallicity distributions in the regions studied. The GCs plotted are all within ~ 20 kpc from the center of NGC 5128 and we are thus comparing clusters in relatively the same projected region as the inner stellar halo. The stellar halo peaks in metallicity near -0.4 dex, coinciding with the major high metallicity peak for GCs. However, $\sim 35\%$ of GCs have $[\text{Z}/\text{H}] < -1$, and only $< 10\%$ of the stellar halo falls in this metal-poor regime, nearly identical to the statistics found by Beasley et al. (2008).

The contrast in metallicity distributions of the stellar and GC population requires explanation. We must be able to show in galaxy formation models why there is such a contrast between two populations that are likely to have formed during the same events of formation. One possibility is destruction efficiency differences between the two populations, where the more metal-rich GCs are destroyed with a higher fraction compared to the metal-poor GCs. However, the destruction of GCs would only dominate in the center regions of the galaxy and there are plenty of metal-rich GCs in the outer halo as well. One could also consider the destruction of metal-poor

GCs being extremely high in the inner halo only. In this scenario, the metal-poor GCs would have to have different structure than the metal-rich GCs which would allow them to be destroyed in the inner regions. This is not supported by the structure of the metal-poor GCs in the outer regions which would have survived, but do not show any major structural differences (Gómez & Woodley 2007).

Another possibility is that the formation efficiency of metal-poor GCs to metal-poor stars is much higher than the formation efficiency of metal-rich GCs to metal-rich stars within the same galaxy (Harris & Harris 2002; Peng et al. 2008). We could also be examining a biased sample of the stellar population. The inner region of the galaxy light is dominated by the metal-rich stellar spheroid, built up by merging events. In this scenario, it may be possible to detect a low metallicity stellar population that formed before or at the onset of hierarchical merging, within pregalactic clouds condensing in the outermost regions of the galaxy. We would expect to find this stellar halo population if we were to examine the stellar halo at much further distances from the center of the galaxy. Studies of M31 (Kalirai et al. 2006) and NGC 3379 (Harris et al. 2007) have shown a transition from a metal-rich to metal-poor stellar population at a galactocentric distance of $12R_{\text{eff}}$. For NGC 5128, this corresponds to a distance of 65 kpc along the isophotal major axis and 45 kpc along the isophotal minor axis, assuming an axial ratio of $b/a = 0.77$. If this transition were detected in NGC 5128 also, it would have strong suggestions for galaxy formation. We hope to conduct an outer-halo search for these low-metallicity stars with upcoming data.

4.6. Alpha-to-Iron Abundance Ratios

The abundance of α -elements compared to that of Fe-type elements can provide information on the formation timescale and chemical history of the gas cloud from which the GCs form. Supernova type II events produce an overabundance of α -elements in relation to Fe-peak elements and occur over a short progenitor lifetime (a few 100 Myr). Supernova type Ia events enrich the interstellar medium after ~ 1 Gyr and produce Fe-peak elements in preference to α -elements. When both type II and Ia (or only type Ia) are occurring the $[\alpha/\text{Fe}]$ ratio decreases. The abundance ratio therefore tells us whether the GCs formed over a long or short timescale (Tornambé & Matteucci 1986) and it also tells us the chemical composition of the cloud at the time of GC formation.

Fig. 10 shows distribution of $[\alpha/\text{Fe}]$ obtained from the SSP models is best fit by a unimodal Gaussian distribution. The NGC 5128 GCs have on average a lower $[\alpha/\text{Fe}]$ than the Milky Way GCs, indicating slower formation times at every given metallicity, as shown in Fig. 13. We also examine age as a function of $[\alpha/\text{Fe}]$ in Fig. 13 and clearly see a wider spread in $[\alpha/\text{Fe}]$ among the older GCs in NGC 5128 than among those with ages < 8 Gyr. A comparable spread is also seen in the Milky Way GCs, however shifted to higher α -element enhancement. The low $[\alpha/\text{Fe}]$ values in the NGC 5128 GCs are seen to occur over their full age range. The GCs in NGC 5128 could have undergone prolonged formation timescales compared to the GCs in other giant systems. The GCs with older ages have a wider spread in $[\alpha/\text{Fe}]$

extending to higher values than GCs with younger ages in NGC 5128. The older GCs within NGC 5128 may have formed within a faster burst or collapse, on average, than the younger GCs within NGC 5128.

5. DISCUSSION

Thus far the ages of GCs determined spectroscopically have made it difficult to support one clear dominant formation scenario for galaxies. The general trend appears to show the majority of GCs in galaxies are old, with spectroscopic ages greater than 8 Gyr from early-type galaxies to dwarf galaxies (Puzia & Sharina 2008; Puzia et al. 2005a; Strader et al. 2005; Kissler-Patig et al. 1998; Frobos et al. 2001). However, some galaxies also have noticeable components of intermediate and young populations of GCs (Mora et al. 2008; Puzia et al. 2005a; Larsen et al. 2003; Strader et al. 2003; Goudfrooij et al. 2001), forming along with perhaps the major starbursting activity in the galaxy. The issue is complicated further by environmental dependencies of GCs. Early-type galaxies, such as giant ellipticals, show a higher relative number of GCs per unit luminosity, the specific frequency (Harris & van den Bergh 1981), than spiral galaxies, which in turn generally have a higher specific frequency than dwarf galaxies (see however Peng et al. 2008, who show that GC fractions for low-mass systems are strongly environmentally dependent). Studies, therefore, tend to concentrate on the most massive galaxies where there is a higher quantity of GCs present, such as this study. These studies are also generally biased towards the brightest and more centrally concentrated GCs in the massive distant early-type galaxies to minimize telescope time and maximize the number of GCs in the sample. This can lead to a spatially biased samples of metal-rich and younger GCs. In the case of NGC 5128, studies with larger, more representative samples of GCs across its entire halo show there is a near 50-50 split between metal-rich and metal-poor GCs (Woodley et al. 2005; Harris et al. 2004) with the metal-rich population being more centrally concentrated than the metal-poor (Beasley et al. 2008; Woodley et al. 2007, 2005; Peng et al. 2004a).

A previous study in NGC 5128 conducted by Peng et al. (2004a) used UVB photometry of GCs obtained with the CTIO 4-meter telescope as well as spectra from the HYDRA instrument to examine GC ages. Although their photometric data suffered from the age-metallicity degeneracy for objects older than 2 Gyr, they were able to show from the photometric indices and the Bruzual & Charlot (1993) models that the metal-poor GCs appear to be between 12-15 Gyr old. They also found 2 young GCs, GC0084 (HGHH-G279) and GC0103 (pff-gc-029), with ages ≤ 1 Gyr, the latter of which is associated with a young, blue tidal stream (Peng et al. 2002). Using spectra obtained with signal-to-noise of at least 40 per resolution element calibrated to the Lick index system, Peng et al. (2004a) compared the measured indices to Thomas et al. (2003) SSP models. Their results indicated that the metal-poor GCs in NGC 5128 have ages ranging between 8-15 Gyr, and the metal-rich GCs have a large range extending between 1-10 Gyr, with 1/3 of their sample greater than 8 Gyr. They also indicate that all the GCs studied have alpha enhancement similar to the Milky Way GCs.

A more recent age, metallicity and alpha-to-iron abundance study of the GCs in NGC 5128 has been performed by Beasley et al. (2008). For 147 GCs extending out to $40'$, they were able to obtain spectra using the 2dF instrument on the AAT with signal-to-noise of 30 per \AA . Their spectra are compared to two sets of SSP models, Lee & Worthey (2005) and Thomas et al. (2003) including the higher-order Balmer line corrections of Thomas et al. (2004). We cannot compare our results directly for GCs in common with Beasley et al. (2008) as age, metallicity, and $[\alpha/\text{Fe}]$ model derived results were not tabulated. They do present empirically derived metallicities for a large fraction of GCs in NGC 5128, however, that are model independent. These are derived from the dependency of known metallicity with Lick index measurements from the Milky Way GCs (please see Beasley et al. 2008, for more details). We have 28 GCs in common with their study (with reasonable uncertainties of $\delta[M/H] < 0.5$) and we plot the comparison in Figure 14. There is scatter about the 1:1 relationship with an rms of 0.25 dex. We can also compare our model derived ages, metallicities, and $[\alpha/\text{Fe}]$ to their graphical results. Their results show that $\sim 85 - 90\%$ of the GC sample is old, with ages similar to the Milky Way GCs. They find an intermediate aged population of 4-8 Gyr that constitutes $\leq 15\%$ of their sample dominated by metal-rich GCs. One very young GC, GC0084 (HGHH-G279) with an age of $\sim 1 - 2$ Gyr was found. The GCs have lower alpha abundances than the Milky Way GCs at a given metallicity.

We find similar results to both previous spectroscopic studies in NGC 5128, although we do not find either as high a fraction of metal-rich GCs with young ages as do Peng et al. (2004a) or as low a fraction of young GCs as Beasley et al. (2008). From our sample, we find 13/72 (18%) of the clusters have ages less than 5 Gyr, and none less than 3.5 Gyr, including GC0084 for which we obtained a more intermediate age of 6.2 ± 0.4 Gyr. All studies do show that the majority of GCs in NGC 5128 have ages greater than 8 Gyr, similar to those in the Milky Way. An important finding, strongly reinforcing that of Beasley et al. (2008), is that a majority of *both* metal-poor (92%) and metal-rich (56%) GCs have old ages. We do not find a strong indication that metal-rich clusters formed exclusively at slightly later times than the metal-poor GCs as suggested by the multiphase in situ scenario (Forbes et al. 1997). However, the range of $[\alpha/\text{Fe}]$ for the old GCs is large, indicating perhaps a range in formation timescale and/or strong chemical variance during the primordial phase. Also the SSP models themselves have limited ability to distinguish between GCs of old ages (see Fig. 7). We also do not find that all metal-rich GCs are old as would be expected in an accretion scenario. In this scenario, the metal-rich GCs are formed in a massive seed galaxy, and metal-poor GCs are accreted through metal-poor dwarfs (Côté et al. 1999, 2000, 2002). But our study indicates a population of intermediate (14%) and younger (18%) GCs, the large majority of which are metal-rich. These younger clusters do not appear to have formed primordially and it seems more probable to suggest they built up by merging events later in the evolutionary history of the galaxy.

The supersolar $[\alpha/\text{Fe}]$ for GCs in NGC 5128 indicates a rapid formation of both metal-rich and metal-poor GCs,

with a mean value of 0.14 ± 0.04 . However, the formation timescales of these GCs are on average slower than those in other elliptical galaxies and more along the lines of spiral and lenticular galaxies (Puzia et al. 2006). In the sparse environment of NGC 5128, the formation of the more metal-rich GCs could be extended over a longer timescale, supported by both the range of ages for the red GCs and the low $[\alpha/\text{Fe}]$ values compared to other giant galaxies.

Different formation scenarios predict different absolute and relative ages of metal-rich and metal-poor GCs. The hierarchical model of accretion and merging of smaller subunits to build larger structures over time suggests that both metal-rich and metal-poor GCs with ages ≥ 9 Gyr might be found in a giant galaxy. The semi-analytic models of Beasley et al. (2002) showed in the hierarchical formation scenario of galaxies that the metal-rich GCs were younger than the metal-poor GCs, with mean ages of 9 and 12 Gyr, respectively. However, extended metal-rich GC formation can take place in the galaxy merging model (Schweizer 1987; Ashman & Zepf 1992) forming GCs down to the present redshift.

On the formation history of GCs, our results indicate that the majority of today's GCS in NGC 5128, both metal-rich and metal-poor, have formed early and are coeval within the uncertainties of our age determinations, likely forming with the bulk of the galaxy field stellar populations. However, this last point is entirely based on integrated-light properties of the diffuse galaxy light as current work with color magnitude diagrams does not go deep enough to reach the main sequence turn-off or sub-giant branch of an intermediate-age sub-population. In any case, we see trends towards younger GC ages with increasing metallicity which is supported by the hierarchical merging scenario.

A formation scenario by Strader et al. (2005), combining the in situ (Forbes et al. 1997) and accretion scenarios (Côté et al. 1999, 2000, 2002), is also consistent with our findings. The metal-poor GCs could have formed in small halos in the early universe until their formation was truncated by the reionization process (Santos 2003). The field stars and metal-rich GCs could then form in massive early-type galaxies. The old ages obtained for the stellar population in the NGC 5128 stellar halo (Rejkuba et al. 2005; Harris 2008) support this scenario as well. In this case, the youngest GCs that are found in NGC 5128 could be produced in more recent merging events.

6. CONCLUSIONS

Using the Gemini South 8-meter telescope with GMOS, we obtained spectra of GCs in NGC 5128 to obtain radial velocities, ages, metallicities, and alpha-to-iron abundance ratios. The main results from this study are:

- We discovered 35 new GCs from radial velocity measurements as well as remeasuring radial velocities for 101 previously confirmed GCs.

- Our quantitative age estimates suggest 68% of our GCs have old ages (> 8 Gyr), 14% have intermediate ages (5 – 8 Gyr), and 18% have young ages (< 5 Gyr), suggesting several, or at least extended, formation epochs.
- Separating the GCs into metal-rich and metal-poor subpopulations by the model-derived $[\text{Z}/\text{H}]$ quantity, we find that 92% of metal-poor ($[\text{Z}/\text{H}] < -1$) and 56% of metal-rich ($[\text{Z}/\text{H}] \geq -1$) GCs in NGC 5128 have ages > 8 Gyr.
- We also find both the Washington color and spectroscopic synthetic metallicity index $[\text{MgFe}]'$ show a bimodal distribution for the GCs, indicating that there are two distinct metallicity subpopulations.
- The $[\alpha/\text{Fe}]$ for the GCs are super solar, but not as large as in the Milky Way. We suggest that the GCs in NGC 5128 formed on slower timescales than GCs in the Milky Way and other massive elliptical galaxies (Puzia et al. 2006).

Our results support a scenario with a rapid, early formation of the bulk of the GCS and significant subsequent major accretion and/or GC- and star-forming events in more recent times. We note that our relatively high fraction of metal-rich and young GCs is likely biased because we probed the inner regions of NGC 5128 and observed mainly the brightest GCs. We consider our results, therefore, to be a fractional upper limit on the number of metal-rich and young GCs in NGC 5128.

Based on observations obtained at the Gemini Observatory, which is operated by the Association of Universities for Research in Astronomy, Inc., with a cooperative agreement with the NSF, on behalf of the Gemini partnership: the National Science Foundation (United States), the Science and Technology Facilities Council (United Kingdom), the National Research Council (Canada), CONICYT (Chile), the Australian Research Council (Australia), Ministério da Ciência e Tecnologia (Brazil) and Ministerio de Ciencia, Tecnología e Innovación Productiva (Argentina). This research used the facilities of the Canadian Astronomy Data Centre operated by the National Research Council of Canada with the support of the Canadian Space Agency. KAW, WEH, and GLHH acknowledge financial support from NSERC. THP acknowledges support from the National Research Council of Canada in form of the Plaskett Fellowship at the Herzberg Institute of Astrophysics. D.G. gratefully acknowledges support from the Chilean *Centro de Astrofísica* FONDAF No. 15010003 and from the Chilean Centro de Excelencia en Astrofísica y Tecnologías Afines (CATA). KAW appreciates the help with Gemini GMOS data reduction provided by Rodrigo Carrasco, Bryan Miller, and Gelys Trancho, and the hospitality of all Gemini South astronomers and staff during a stay at the Gemini South facilities in 2006.

REFERENCES

- Arimoto, N. & Yoshii, Y. 1987, *A&A*, 173, 23
 Ashman, K. M., & Zepf, S. E. 1992, *ApJ*, 384, 50
 Barbuy, B., Bica, E., & Ortolani, S. 1998, *A&A*, 333, 117
 Baugh, C. M., Cole, S., Frenk, C. S., & Lacey, C. G. 1998, *ApJ*, 498, 504
 Beasley, M. A., Bridges, T., Peng, E. W., Harris, W. E., Harris, G. L. H., Forbes, D. A., & Mackie, G. 2008, *MNRAS*, 386, 1443

- Beasley, M. A., Baugh, C. M., Frobes, D. A., Sharples, R. M., & Frenk, C. S. 2002, *MNRAS*, 333, 383
- Beaulieu, S. F., Gilmore, G., Elson, R. A. W., Johnson, R. A., Santiago, B., Sigurdsson, S., & Tanvir, N. 2001, *AJ*, 121, 2618
- Brodie, J. P., Strader, J., Denicolò G., Beasley, M. A., Cenarro, A. J., Larsen, S. S., Kuntschner, H., & Forbes, D. A. 2005, *AJ*, 129, 2643
- Bruzual, A. G. & Charlot, S. 1993, *ApJ*, 405, 588
- Burstein, D., Faber, S. M., Gaskell, C. M., & Krumm, N. 1984, *ApJ*, 287, 586
- Cantiello, M. & Blakeslee, J. P. 2007, *ApJ*, 669, 982
- Cenarro, A. J., Cervantes, J. L., Beasley, M. A., Marín-Franch, A., & Vazdekis, A. 2009, *ApJ*, 689, 29
- Cole, S., Lacey, C. G., Baugh, C. M., & Frenk, C. S. 2000, *MNRAS*, 319, 168
- Côté, P., Marzke, R. O., & West, M. J. 1998, *ApJ*, 501, 554
- Côté, P., Marzke, R. O., West, M. J., & Minniti, D. 2000, *ApJ*, 533, 869
- Côté, P., West, M. J., & Marzke, R. O. 2002, *ApJ*, 567, 853
- Djorgovski, S. & Davis, M. 1987, *ApJ*, 313, 59
- Dressler, A., Lynden-Bell, D., Burstein, D., Davies, R. L., Faber, S. M., Terlevich, R., & Wegner, G. 1987, *ApJ*, 313, 42
- Eggen, O. J., Lynden-Bell, D., & Sandage, A. R. 1962, *ApJ*, 136, 748
- Ferrarese, L., Mould, J. R., Stetson, P. B., Tonry, J. L., Blakeslee, J. P., & Ajhar, E. A. 2007, *ApJ*, 654, 186
- Forbes, D. A., Brodie, J. P., & Grillmair, C. J. 1997, *AJ*, 113, 1652
- Forbes, D. A., Beasley, M. A., Brodie, J. P., & Kissler-Patig, M. 2001, *ApJ*, 563, L143
- Gómez, M. & Woodley, K. A. 2007, *ApJ*, 670, L105
- Goudfrooij, P., Mack, J., Kissler-Patig, M., Meylan, G., & Minniti, D. 2001, *MNRAS*, 322, 643
- Graham, J. A. 1998, *ApJ*, 502, 245
- Harris, W. E. & van den Bergh, S. 1981, *AJ*, 86, 1627
- Harris, G. L. H., & Harris, W. E. 2000, *AJ*, 120, 2423
- Harris, W. E., & Harris, G. L. H. 2002, *AJ*, 123, 3108
- Harris, G. L. H., Harris, W. E., & Geisler, D. 2004, *AJ*, 128, 723
- Harris, G. L. H., Schmidt, B. P., Hesser, J. E., Reid, M., Milne, M., Hulme, S. C., & Kidd, T. T. 2004, *AJ*, 128, 712
- Harris, W. E., Harris, G. L. H., Layden, A. C., & Wehner, E. M. H. 2007, *ApJ*, 666, 903
- Harris, W. E. 2008, MPA/ESO/MPE/USM Joint Astronomy Conference, Chemical Evolution of Dwarf Galaxies and Stellar Clusters.
- Harris, G. L. H., Rejkuba, M., & Harris, W. E. 2009, submitted to *PASA*
- Hempel, M., Hilker, M., Kissler-Patig, M., Puzia, T. H., Minniti, D., & Goudfrooij, P. 2003, *A&A*, 405, 487
- Hempel, M., Kissler-Patig, M., Puzia, T. H., & Hilker, M. 2007, *A&A*, 463, 493
- Kalirai, J. S., Gilbert, K. M., Guhathakurta, P., Majewski, S. R., Ostheimer, J. C., Rich, R. M., Cooper, M. C., Reitzel, D. B., & Patterson, R. J. 2006, *ApJ*, 648, 389
- Kauffmann, G., White, S. D., & Guiderdone, B. 1993, *MNRAS*, 264, 201
- King, I. R. 1962, *AJ*, 67, 471
- Kissler-Patig, M., Brodie, J. P., Schroder, L. L., Forbes, D. A., Grillmair, C. J., & Huchra, J. P. 1998, *AJ*, 115, 105
- Kundu, A., Zepf, S. E., Hempel, M., Morton, D., Ashman, K. M., Maccarone, T. J., Kissler-Patig, M., Puzia, T. H., & Vesperini, E. 2005, *ApJ*, 634, L41
- Larsen, S. S. 1999, *A&AS*, 139, 393
- Larsen, S. S. 2001, *AJ*, 122, 1782
- Larsen, S. S., Brodie, J. P., Beasley, M. A., Forbes, D. A., Kissler-Patig, M., Kuntschner, H., & Puzia, T. H. 2003, *ApJ*, 585, 767
- Larson, R. B. 1974, *MNRAS*, 166, 585
- Larson, R. B. 1975, *MNRAS*, 173, 671
- Lee, H.-c. & Worthey, G. 2005, *ApJS*, 160, 176
- Malin, D. R. 1978, *Nature*, 276, 591
- Marín-Franch, A., Aparicio, A., Piotto, G., Rosenberg, A., Chaboyer, B., Sarajedini, A., Siegel, M., Anderson, J., Bedin, L. R., Dotter, A., Hempel, M., King, I., Majewski, S., Milone, A. P., Paust, N., & Reid, I. N. 2008, *ApJ*, 694, 1498
- Mendel, J. T., Proctor, R. N. & Forbes, D. A. 2007, *MNRAS*, 379, 1618
- Mora, M. D., Larsen, S. S. & Kissler-Patig, M. *A&A*, 2008, 489, 1065
- Mould, J. & Aaronson, M. 1980, *ApJ*, 240, 464
- Ortolani, S., Renzini, A., Gilmozzi, R., et al. 1995, *Nature*, 377, 701
- Parratt, L. G. 1961, *Probability and Experimental Errors in Science: An Elemental Survey* (John Wiley & Sons Inc., New York and London)
- Peebles, P. J. E. 1980, *The Large-Scale Structure of the Universe* (Princeton: Princeton University Press)
- Peng, E. W., Ford, H. C., Freeman, K. C., & White, R. L. 2002, *AJ*, 124, 3144
- Peng, E. W., Ford, H. C., & Freeman, K. C. 2004a, *ApJ*, 602, 705
- Peng, E. W., Ford, H. C., & Freeman, K. C. 2004b, *ApJS*, 150, 367
- Peng, E. W., Jordán, A., Côté, P., Takamiya, M., West, M. J., Blakeslee, J. P., Chen, C.-W., Ferrarese, L., Mei, S., Tonry, J. L. & West, A. A. 2008, *ApJ*, 681, 197
- Pipino, A. & Matteucci, F. 2004, *MNRAS*, 172, 968
- Pipino, A., Matteucci, F., & Chiappini, C. 2006, *ApJ*, 638, 739
- Pipino, A., Puzia, T. H., & Matteucci, F. 2007, *ApJ*, 665, 295
- Puzia, T. H. 2003, PhD thesis, Ludwig-Maximilians-Universitaet Muenchen
- Puzia, T. H., Zepf, S. E., Kissler-Patig, M., Hilker, M., Minniti, D., & Goudfrooij, P. 2002, *A&A*, 391, 453
- Puzia, T. H., Kissler-Patig, M., Thomas, D., Maraston, C., Saglia, R. P., Bender, R., Goudfrooij, P., & Hempel, M. 2005a, *A&A*, 439, 997
- Puzia, T. H., Perrett, K. M., & Bridges, T. J. 2005b, *A&A*, 434, 909
- Puzia, T. H., Kissler-Patig, M., & Goudfrooij, P. 2006, *ApJ*, 648, 383
- Puzia, T. H., & Sharina, M. E. 2008, *ApJ*, 674, 909
- Rejkuba, M., Greggio, L., Harris, W. E., Harris, G. L. H., & Peng, E. W. 2005, *ApJ*, 631, 262
- Santos, M. R. 2003, in Proc. ESO Workshop, Extragalactic Globular Cluster Systems (Berlin: Springer), 348
- Schiavon, R. P., Rose, J. A., Courteau, S., & MacArthur, L. A. 2005, *ApJS*, 160, 163
- Schweizer F. 1987, in Proc. Eighth Santa Cruz Summer Workshop in Astronomy and Astrophysics, Nearly Normal Galaxies: From the Planck Time to the Present (New York: Springer), 18
- Sharina, M. E., Afanasiev, V. L., & Puzia, T. H. 2006, *MNRAS*, 372, 1259
- Silk, J. 1977, *ApJ*, 214, 152
- Somerville, R. S., Primack, J. R., & Faber, S. M. 2001, *MNRAS*, 320, 504
- Spergel, D. N., et al. 2003, *ApJS*, 148, 175
- Spitler, L., Forbes, D. A., & Beasley, M. A. 2008, *MNRAS*, 389, 1150
- Strader, J., Brodie, J. P., Schweizer, F., Larsen, S. S., & Seitzer, P. 2003, *AJ*, 125, 626
- Strader, J., Brodie, J. P., Cenarro, A. J., Beasley, M. A., & Forbes, D. A. 2005, *AJ*, 130, 1315
- Tinsley, B. M. 1972, *ApJ*, 178, 319
- Thomas, D., Maraston, C., & Bender, R. 2003, *MNRAS*, 339, 897
- Thomas, D., Maraston, C., & Korn, A. 2004, *MNRAS*, 351, L19
- Toomre, A. 1997, *The Evolution of Galaxies and Stellar Populations*, ed. B. Tinsley & R. B. Larson (New Haven: Yale University Obs.), 401
- Tornambé, A. & Matteucci, F. 1986, *MNRAS*, 223, 69
- Trager, S. C., Worthey, G., Faber, S. M., Burstein, D., & Gonzalez, J. J. 1998, *ApJS*, 116, 1
- Trancho, G., Bastian, N., Miller, B. W., & Schweizer, F. 2007, *ApJ*, 664, 284
- Treu, T., Stiavelli, M., Casertano, S., Møller, P., & Bertin, G. 1999, *MNRAS*, 308, 1037
- Tropicco, M. J. & Bell, R. A. 1995, *AJ*, 110, 3035
- van Dokkum, P. G. 2001, *PASP*, 113, 1420
- White, S. D. & Frenk, C. S. 1991, *ApJ*, 379, 52
- White, S. D. & Rees, M. J. 1978, *MNRAS*, 183, 341
- Whitmore, B. C. & Schweizer, F. 1995, *AJ*, 109, 960
- Woodley, K. A., Harris, W. E., & Harris, G. L. H., 2005, *AJ*, 129, 2654
- Woodley, K. A., Harris, W. E., Beasley, M. A., Peng, E. W., Bridges, T. J., Forbes, D. A., & Harris, G. L. H. 2007, *AJ*, 134, 494
- Woodley, K. A., Gómez, M., Harris, W. E., Geisler, D., & Harris, G. L. H., 2009, *AJ*, submitted
- Worthey, G. 1994, *ApJS*, 95, 107
- Worthey, G. & Ottaviani, D. L. 1997, *ApJS*, 111, 377
- Worthey, G., Faber, S. M., Gonzalez, J. J., & Burstein, D. 1994, *ApJS*, 94, 687
- Yoon, S.-J., Yi, S. K., & Lee, Y.-W., 2006, *Sci*, 111, 1129

TABLE 1
GEMINI-SOUTH GMOS OBSERVATION DATA SUMMARY

Field	Field Center (J2000)	Time (hr)	Year	N Objects Observed
1	13 25 42.5 -42 58 05.9	3.75	2005	23
2	13 24 56.4 -42 58 04.8	3	2005	19
3	13 24 57.6 -43 04 55.2	3.5	2005	23
4	13 25 45.6 -43 06 00.0	3.5	2005	18
5	13 25 54.0 -42 58 21.8	3	2007	25
6	13 25 20.0 -42 57 23.0	3	2007	22
7	13 24 55.0 -43 00 32.4	3	2007	25
8	13 25 16.4 -43 05 43.4	3	2007	21

TABLE 2
NEW RADIAL VELOCITY MEASUREMENTS OF KNOWN GLOBULAR CLUSTERS

GC Name	Old GC Name	RA (J2000)	Decl. (J2000)	Mask & Slit	S/N ^a (\AA^{-1})	$v_{r,GMOS}$ (km s^{-1})	v_r (km s^{-1})
GC0046	pff_gc-015	13 24 41.20	-43 01 45.6	m=7 s=17	54	508±31	518±18
GC0049	pff_gc-017	13 24 43.63	-42 58 16.4	m=2 s=01	54	442±53	717±36
GC0050	WHH-5	13 24 44.58	-43 02 47.3	m=3 s=03	47	716±32	718±16
				m=7 s=22	37	735±26	
GC0052	AAT109711	13 24 45.35	-42 59 33.5	m=2 s=02	66	167±73	210±33
				m=7 s=09	60	186±48	
GC0053	AAT109788	13 24 45.78	-43 02 24.5	m=3 s=02	27	471±47	504±17
				m=7 s=23	20	508±26	
GC0056	pff_gc-018	13 24 47.10	-43 06 01.7	m=3 s=01	27	500±30	528±12
GC0057	G277	13 24 47.37	-42 58 29.8	m=2 s=04	59	714±31	728±18
				m=7 s=08	50	761±33	
GC0062	pff_gc-019	13 24 48.97	-42 57 48.4	m=2 s=05	66	588±46	602±23
GC0065	pff_gc-020	13 24 50.48	-42 59 49.0	m=2 s=06	52	250±48	291±33
GC0068	C100	13 24 52.06	-43 04 32.7	m=3 s=10	63	195±29	195±29
GC0070	G302	13 24 53.29	-43 04 34.8	m=3 s=09	86	482±31	485±23
GC0073	pff_gc-022	13 24 54.33	-43 03 15.5	m=3 s=07	138	557±60	596±35
GC0077	C11	13 24 54.73	-43 01 21.7	m=7 s=15	40	746±10	792± 1
GC0078	AAT111406	13 24 55.29	-43 03 15.6	m=3 s=08	30	552±31	568±28
GC0084	G279	13 24 56.27	-43 03 23.4	m=3 s=11	203	226±91	348±31
GC0086	C31	13 24 57.44	-43 01 08.1	m=7 s=14	34	687±11	685± 9
GC0087	G369	13 24 57.52	-42 59 23.3	m=7 s=06	55	481±22	500±13
GC0088	pff_gc-025	13 24 57.56	-43 05 32.8	m=3 s=12	35	864±30	893±21
GC0091	C3	13 24 58.21	-42 56 10.0	m=2 s=07	35	507±30	562± 2
GC0098	pff_gc-027	13 25 00.64	-43 05 30.3	m=3 s=14	39	496±30	503±21
GC0105	pff_gc-030	13 25 01.73	-43 00 09.9	m=2 s=16	22	306±48	343±24
GC0109	G176	13 25 03.13	-42 56 25.1	m=2 s=12	44	480±30	540±11
GC0110	G066	13 25 03.18	-43 03 02.5	m=7 s=25	35	572±15	571± 6
				m=3 s=15	40	515±27	
GC0116	AAT112752	13 25 04.12	-43 00 19.6	m=2 s=15	27	733±54	716±45
GC0120	WHH-7	13 25 05.02	-42 57 15.0	m=2 s=13	41	639±24	687±15
GC0121	G035	13 25 05.29	-42 58 05.8	m=7 s=01	30	804±30	787±19
GC0124	G342	13 25 05.83	-42 59 00.6	m=2 s=14	43	481±27	526±16
GC0127	AAT113428	13 25 07.33	-43 06 20.6	m=3 s=17	63	700±36	727±22
				m=8 s=05	36	767±33	
GC0129	WHH-8	13 25 07.62	-43 01 15.2	m=7 s=12	33	666±21	673±18
GC0130	WHH-9	13 25 08.51	-43 02 57.4	m=3 s=16	40	284±28	295±23
GC0132	pff_gc-038	13 25 08.82	-43 04 14.9	m=8 s=15	32	436±16	433±12
GC0134	K-029	13 25 09.19	-42 58 59.2	m=7 s=04	41	630±33	646±26
GC0137	K-033	13 25 10.25	-42 55 09.5	m=6 s=03	29	576±14	576±12
GC0143	pff_gc-041	13 25 11.17	-43 03 09.6	m=3 s=21	105	381±39	426±21
GC0145	G081	13 25 12.11	-42 57 25.2	m=6 s=14	46	489±25	500±21
GC0150	R261	13 25 12.90	-43 07 59.1	m=8 s=01	47	633± 9	619± 3
GC0154	R259	13 25 13.88	-43 07 32.5	m=8 s=04	19	621±38	623±29
GC0158	WHH-11	13 25 14.24	-43 07 23.5	m=8 s=03	31	637±23	616±18
GC0161	AAT114769	13 25 15.12	-42 57 45.7	m=6 s=15	29	541±61	553±57
GC0164	AAT114913	13 25 15.93	-43 06 03.3	m=8 s=09	29	573±38	570±32
GC0165	pff_gc-049	13 25 16.06	-43 05 06.5	m=8 s=10	44	726±24	707±19
GC0186	R247	13 25 19.99	-43 07 44.1	m=8 s=02	18	723±33	703±27
GC0188	AAT115679	13 25 20.72	-43 06 35.9	m=8 s=06	31	846±50	817±47
GC0193	C143	13 25 23.20	-43 03 12.9	m=8 s=21	14	328±81	328±81
GC0197	WHH-14	13 25 25.49	-42 56 31.2	m=6 s=08	46	604±52	597±34
GC0199	pff_gc-052	13 25 25.75	-43 05 16.5	m=8 s=12	41	576±39	534±31
GC0205	WHH-16	13 25 27.97	-43 04 02.2	m=8 s=16	28	715±14	710±13
GC0208	WHH-17	13 25 29.25	-42 57 47.1	m=1 s=07	100	658±32	644±26
GC0210	G169	13 25 29.43	-42 58 09.9	m=1 s=17	27	660±34	649±16
				m=6 s=17	26	653±35	
GC0211	pff_gc-053	13 25 29.62	-42 54 44.5	m=6 s=01	27	390±18	411±13
GC0215	WHH-18	13 25 30.07	-42 56 46.9	m=6 s=07	40	761±13	759±11
GC0226	AAT117322	13 25 31.73	-42 55 15.7	m=6 s=02	33	245±56	303±51
GC0230	G359	13 25 32.42	-42 58 50.2	m=1 s=16	36	497±26	494±20
GC0231	pff_gc-056	13 25 32.80	-42 56 24.4	m=6 s=06	88	254±33	284±21
GC0232	R223	13 25 32.80	-43 07 02.2	m=4 s=04	56	766±23	775± 1
GC0233	K-131	13 25 32.88	-43 04 29.2	m=4 s=12	32	607±23	613±20
GC0238	G206	13 25 34.10	-42 59 00.7	m=6 s=21	37	716±34	639±19
GC0239	C45	13 25 34.25	-42 56 59.1	m=1 s=06	68	591±39	600±23
				m=6 s=05	48	621±61	
GC0243	C154	13 25 34.71	-43 03 30.2	m=4 s=18	34	719±86	719±86
GC0245	pff_gc-058	13 25 35.12	-42 56 45.3	m=1 s=04	119	284±36	344±16
GC0248	WHH-22	13 25 35.31	-43 05 29.0	m=4 s=08	60	599±17	597±16
GC0249	MAGJM-08	13 25 35.50	-42 59 35.2	m=1 s=22	36	730±31	714±20
GC0255	AAT118198	13 25 37.47	-43 05 44.9	m=4 s=09	27	524±18	534±16
GC0265	C17	13 25 39.73	-42 55 59.2	m=1 s=01	61	715±25	781± 2
GC0266	C18	13 25 39.88	-43 05 01.9	m=4 s=11	66	442± 7	477± 2
GC0272	R203	13 25 40.90	-43 08 16.0	m=4 s=02	43	409±72	446±31
GC0273	AAT118874	13 25 41.36	-42 58 08.9	m=5 s=11	26	821±39	774±35
GC0277	G370	13 25 42.25	-42 59 17.0	m=1 s=12	70	471±24	477±14
				m=5 s=08	62	471±21	

TABLE 3
RADIAL VELOCITY MEASUREMENTS OF NEW GLOBULAR CLUSTERS

GC Name	RA (J2000)	Decl. (J2000)	Mask & Slit	S/N ^a (\AA^{-1})	$v_{r,GMOs}$ (km s^{-1})	C (mag)	σ C (mag)	M (mag)	σ M (mag)	T_1 (mag)	σ T_1 (mag)
GC0445	13 24 40.45	-43 01 56.9	m=7 s=24	16	504±45	21.86	0.03	20.93	0.02	20.04	0.03
GC0446	13 24 50.43	-43 04 51.0	m=3 s=05	30	358±27	21.27	0.01	20.08	0.01	19.09	0.01
GC0447	13 24 50.90	-42 59 59.0	m=7 s=11	07	607±77	22.42	0.03	21.90	0.02	20.73	0.02
GC0448	13 24 53.64	-42 57 59.3	m=7 s=03	15	623±53	22.12	0.03	21.16	0.02	20.22	0.02
GC0449	13 24 53.96	-43 00 43.4	m=7 s=16	18	332±42	21.79	0.04	20.63	0.03	19.71	0.04
GC0450	13 24 54.97	-43 02 52.4	m=7 s=21	25	415±92	21.37	0.05	21.03	0.04	19.08	0.02
GC0451	13 24 55.42	-42 59 49.0	m=2 s=10 m=7 s=07	41 36	675±42 ^b	20.89	0.03	20.14	0.03	19.69	0.03
GC0452	13 24 57.74	-42 58 51.8	m=7 s=10	11	645±88	22.24	0.01	21.50	0.01	20.71	0.01
GC0453	13 24 58.57	-42 58 16.2	m=7 s=02	35	626±14	20.34	0.01	19.29	0.02	18.40	0.01
GC0454	13 25 02.78	-43 02 04.0	m=7 s=19	28	352±64	21.15	0.05	20.35	0.06	19.37	0.09
GC0455	13 25 05.02	-43 01 33.6	m=7 s=13	23	480±57	21.83	0.02	20.94	0.02	19.37	0.02
GC0456	13 25 06.72	-42 59 16.6	m=7 s=05 m=6 s=22	44 64	401±27 ^c	19.73	0.07	18.98	0.06	18.84	0.06
GC0457	13 25 06.82	-42 57 32.1	m=2 s=19	32	550±43	21.49	0.01	20.40	0.01	19.49	0.01
GC0458	13 25 07.68	-42 55 49.5	m=6 s=12	17	559±64	21.73	0.02	21.34	0.01	20.85	0.01
GC0459	13 25 17.63	-42 56 14.4	m=6 s=11	09	458±72	22.97	0.04	22.39	0.03	21.29	0.02
GC0460	13 25 20.45	-43 06 09.4	m=8 s=07	32	743±42	21.80	0.03	20.75	0.02	19.85	0.02
GC0461	13 25 23.99	-43 03 45.1	m=8 s=20	17	527±74	21.74	0.04	21.14	0.03	20.23	0.03
GC0462	13 25 25.99	-43 03 25.9	m=8 s=18	39	269±27	19.77	0.01	19.30	0.02	18.64	0.22
GC0463	13 25 27.28	-42 58 28.8	m=6 s=19	25	227±36	21.06	0.01	20.00	0.02	19.15	0.01
GC0464	13 25 27.45	-42 55 30.9	m=6 s=10	14	475±78	22.23	0.04	22.61	0.04	20.72	0.02
GC0465	13 25 30.22	-43 06 54.0	m=8 s=08	15	642±58	22.86	0.03	21.82	0.03	21.16	0.02
GC0466	13 25 30.37	-43 05 42.5	m=8 s=11	14	379±50	21.68	0.02	21.03	0.01	19.76	0.01
GC0467	13 25 30.96	-42 58 36.9	m=6 s=18	26	209±33	20.91	0.02	20.85	0.02	19.24	0.01
GC0468	13 25 31.27	-42 55 47.6	m=1 s=02	32	372±68	22.89	0.03	21.93	0.04	21.01	0.02
GC0469	13 25 31.73	-42 59 57.4	m=1 s=21	20	377±39	-	-	-	-	-	-
GC0470	13 25 33.14	-42 54 57.6	m=6 s=04	16	624±74	22.02	0.02	21.39	0.02	20.72	0.02
GC0471	13 25 42.11	-42 57 23.9	m=5 s=13	28	190±45	20.61	0.06	20.06	0.05	19.54	0.02
GC0472	13 25 42.98	-43 00 00.2	m=1 s=20	44	306±64	-	-	25.08	0.38	24.01	0.53
GC0473	13 25 43.01	-43 00 07.4	m=5 s=09	19	318±71	22.04	0.03	21.36	0.02	20.41	0.03
GC0474	13 25 44.67	-42 58 24.0	m=5 s=19	26	376±75	21.39	0.04	21.34	0.07	19.93	0.02
GC0475	13 25 46.36	-43 04 44.6	m=4 s=15	21	550±55	-	-	-	-	-	-
GC0476	13 25 47.15	-42 57 48.9	m=5 s=15	62	482±45	20.53	0.02	19.93	0.01	19.33	0.01
GC0477	13 25 47.83	-42 57 32.6	m=1 s=08	15	335±66	23.17	0.05	22.14	0.04	21.27	0.04
GC0478	13 25 49.24	-43 00 01.8	m=5 s=04	56	465±30	20.20	0.02	19.47	0.02	18.84	0.01
GC0479	13 26 00.00	-42 59 58.1	m=5 s=10	14	525±86	22.02	0.03	21.51	0.03	20.81	0.02

^aApproximate S/N is measured per \AA between 4700 \AA - 4830 \AA .

^bThe quoted radial velocity is a weighted average. The individual measurements were 655±69 for m=2,s=10 and 687±52 for m=7,s=07.

^cThe quoted radial velocity is a weighted average. The individual measurements were 410±46 for m=7,s=05 and 398±34 for m=6,s=22.

TABLE 4 — *Continued*

GC Name	H δ_A (Å)	H δ_F (Å)	CN ₁ (mag)	CN ₂ (mag)	Ca4227 (Å)	G4300 (Å)	H γ_A (Å)	H γ_F (Å)	Fe4383 (Å)	Ca4455 (Å)	Fe4531 (Å)	C ₂ 4668 (Å)	H β (Å)	Fe5015 (Å)	Mg ₁ (mag)	Mg ₂ (mag)	Mg _b (Å)	Fe5270 (Å)	Fe5335 (Å)	Fe5406 (Å)
GC0455	-1.6306	0.8084	0.0731	0.0506	0.2824	5.1248	0.7794	2.3058	5.5051	-1.1745	0.8106	1.3695	2.3412	3.0716	-	-	2.5287	-1.8059	-	-
GC0456	2.1452	2.8832	-0.0540	-0.0061	0.7633	2.3089	0.9480	1.7331	1.4008	0.5068	1.0851	1.2455	2.1553	3.6471	0.0404	0.0805	1.3097	1.3463	1.0543	-0.0226
GC0457	-2.3913	0.8087	0.1319	0.1733	1.3580	5.3653	-3.8280	-2.1089	4.5896	1.2576	4.7112	3.8290	1.3674	4.3891	0.0820	0.2400	3.0944	3.2153	2.5785	2.0803
GC0458	5.6391	5.0668	-0.1986	-0.1477	0.7800	-1.7344	7.1554	5.4226	-0.0642	-0.0442	3.4808	-2.1540	7.2452	4.2332	-0.0292	0.0589	2.0766	2.6270	0.0727	0.6684
GC0459	-4.5714	-4.1819	0.0940	0.0038	-4.6136	17.6375	-10.700	2.5519	3.8874	-1.1577	-1.4187	0.5869	4.6120	3.0126	0.0225	0.1625	4.6276	1.4509	-0.3355	2.3666
GC0460	0.0712	-0.0573	0.1012	0.0344	0.7402	8.1765	-3.7429	-0.8602	3.3015	0.5762	2.9212	-8.0282	1.7112	1.6921	0.0668	0.1794	3.2792	2.2401	2.7443	1.8727
GC0461	3.4267	2.7558	0.0199	0.0333	0.4209	2.2199	0.2039	1.9455	7.9228	-0.1062	2.0934	-2.5531	1.9495	-2.5294	-0.0025	0.0664	0.6908	1.7830	1.1241	0.8945
GC0462	0.5852	1.9308	-0.0023	-0.0029	0.2001	2.5730	-0.3080	1.8920	1.1552	-0.0661	1.0498	-0.2565	2.3923	2.2879	0.0103	0.0632	1.4136	1.1306	0.9843	0.5731
GC0463	-3.5426	2.2641	0.1392	0.0917	1.8813	4.8507	-0.3654	1.1208	2.9660	1.2240	3.0995	4.8778	1.4706	3.7267	0.0829	0.2112	2.3271	2.4680	2.1291	1.6496
GC0464	-1.8861	2.0097	0.0966	0.1593	0.1606	0.2545	-4.3895	-0.7635	0.6148	-0.4127	3.6530	0.3468	2.6733	1.9231	0.0623	0.1053	1.5730	1.6934	2.0778	1.3158
GC0465	-9.4001	0.0241	0.1366	0.2583	1.2805	0.4874	-2.3828	1.0598	0.9909	-3.8063	0.5461	8.9501	2.0939	3.8978	0.0280	0.1189	1.7690	2.2560	2.3308	0.8988
GC0466	-0.8225	3.7125	0.0259	-0.0080	-0.8623	3.7416	5.1444	1.9121	0.1162	0.6158	2.3228	2.5484	1.0259	2.9599	-0.0118	0.0524	0.4343	2.1719	1.2911	0.9803
GC0467	-1.2462	-1.4552	0.0383	0.1177	1.7722	5.4448	-4.1422	-1.6381	0.9092	-0.2114	2.6409	2.1461	1.4025	3.4334	0.0684	0.2005	3.0327	2.5884	2.5033	1.5173
GC0467	-0.5111	0.6348	0.1512	0.2041	1.1294	4.2834	-3.6911	-0.5021	1.4997	1.3433	2.2947	3.1043	1.6962	3.1962	-	-	2.4749	-	-	-
GC0469	-3.0783	0.7529	0.1512	0.1982	1.2378	6.4325	-3.5685	-3.7806	3.7180	0.1960	2.1617	4.4523	1.7565	7.2461	0.0877	0.2526	4.0168	3.0650	3.5450	2.1528
GC0470	-0.1805	2.9322	0.1537	0.1366	-0.9027	3.1648	3.8615	4.3280	0.8569	-2.5320	4.8058	6.7715	4.7605	6.0953	-	-	-	-	-	-
GC0471	4.0864	4.7551	-0.0067	0.0343	-0.2654	1.8684	4.6994	3.8730	-0.1454	0.6803	3.1311	3.4185	4.1591	3.9997	-	-	1.7942	-	-	-
GC0472	2.8577	3.4811	0.0110	0.0674	0.1896	1.2915	0.8363	0.7698	1.6225	1.0304	1.1597	0.6862	2.8235	3.4633	0.0431	0.1136	2.0947	1.5646	1.3565	0.8709
GC0473	-0.9468	3.4143	0.0038	0.0172	1.7881	6.7347	-0.0588	-0.0131	-2.8787	-0.7121	1.9487	-3.0266	2.2980	4.2900	-	-	3.0592	-	-	-
GC0474	0.6447	1.6260	-0.0740	-0.0286	0.6804	1.2002	4.5377	7.4150	-9.9251	1.4992	1.3297	2.5528	1.9628	1.6762	-0.0705	-0.0386	1.7178	1.3577	-4.2383	-
GC0475	2.9993	4.4142	-0.0631	0.0959	0.6911	5.8976	-6.9253	1.4080	6.5623	2.3295	2.3263	3.5092	1.7689	5.1894	0.0721	0.2169	3.2248	2.0129	2.6856	1.5238
GC0476	2.1385	3.4857	-0.0683	-0.0155	-0.6223	1.1330	1.5974	2.2733	0.9937	0.2742	0.8316	1.1571	2.3315	0.8942	0.0412	0.0606	0.5055	0.6597	0.7208	0.4178
GC0477	-0.4655	-0.2545	0.0773	0.0699	0.8937	5.4502	-2.7529	-0.8308	3.5067	0.0833	0.9955	8.0893	1.9719	6.1703	0.1019	0.2818	4.3928	1.6664	2.7444	2.3220
GC0478	1.7881	2.5779	-0.0239	0.0319	-0.1879	3.7636	1.0490	1.2397	1.2958	0.4557	2.0493	0.1850	2.0022	1.6836	0.0324	0.0847	1.0199	1.1461	1.0334	0.3661
GC0479	2.4254	1.9427	-0.0011	-0.0970	-0.5742	3.9976	1.6516	2.0486	0.1615	2.7191	0.6059	3.8250	2.3190	4.0115	0.0579	0.0807	-0.9380	-2.2628	1.4383	1.2572

TABLE 5
LICK INDICES UNCERTAINTIES FOR GLOBULAR CLUSTERS IN NGC 5128

GC Name	H δ_A (\AA)	H δ_F (\AA)	CN ₁ (mag)	CN ₂ (mag)	Ca4227 (\AA)	G4300 (\AA)	H γ_A (\AA)	H γ_F (\AA)	Fe4383 (\AA)	Ca4455 (\AA)	Fe4531 (\AA)	C ₄ 668 (\AA)	H β (\AA)	Fe5015 (\AA)	Mg ₁ (mag)	Mg ₂ (mag)	Mg _b (\AA)	Fe5270 (\AA)	Fe5335 (\AA)	Fe5406 (\AA)
GC0046	0.0315	0.0180	0.0009	0.0012	0.0185	0.0617	0.0436	0.0240	0.1045	0.0283	0.0514	0.0667	0.0282	0.0682	0.0006	0.0006	0.0613	0.0894	0.0420	0.0289
GC0049	0.3988	0.1915	0.0080	0.0104	0.1605	0.4021	0.2501	0.2194	0.5541	0.2638	0.6326	0.5825	0.2701	0.5488	0.0066	0.0070	0.2338	0.2638	0.2725	0.2492
GC0050	0.0354	0.0253	0.0020	0.0024	0.0311	0.0678	0.0515	0.0232	0.0812	0.0339	0.0473	0.0724	0.0496	0.0489	0.0005	0.0007	0.0446	0.0268	0.0290	0.0271
GC0052	0.1512	0.1165	0.0062	0.0084	0.1218	0.3424	0.1615	0.1273	0.2711	0.1386	0.4907	0.6585	0.3217	0.5554	0.0048	0.0051	0.1610	0.2058	0.3869	0.2480
GC0053	0.2361	0.1861	0.0066	0.0087	0.1154	0.1796	0.3988	0.1371	0.3084	0.1169	0.1893	0.5849	0.1345	0.5756	-	-	-	-	-	-
GC0056	0.2413	0.1032	0.0068	0.0040	0.0511	0.0761	0.1034	0.0777	0.1357	0.0547	0.0989	0.2055	0.0582	0.1830	0.0021	0.0020	0.0585	0.0507	0.0805	0.0742
GC0057	0.2027	0.1361	0.0059	0.0067	0.1264	0.1885	0.2396	0.1768	0.3815	0.1981	0.3174	0.7393	0.1897	0.3978	0.0052	0.0057	0.2627	0.2080	0.1744	0.2031
GC0062	0.2027	0.1361	0.0116	0.0142	0.1463	0.3201	0.3590	0.1370	0.4307	0.2213	0.4136	0.6322	0.1506	0.7987	0.0035	0.0040	0.1805	0.4216	0.3824	0.1885
GC0065	0.3056	0.2118	0.0110	0.0127	0.2356	0.5538	0.3199	0.3013	0.7883	0.3454	0.7750	1.1288	0.4606	0.6548	0.0065	0.0084	0.2665	0.2877	0.4926	0.2333
GC0068	0.1106	0.1388	0.0060	0.0079	0.0658	0.1321	0.1270	0.1458	0.2236	0.1030	0.1604	0.2270	0.1505	0.2426	0.0025	0.0072	0.0959	0.1428	0.2724	0.1497
GC0070	0.0774	0.0527	0.0025	0.0028	0.0511	0.1357	0.0993	0.0591	0.2356	0.0664	0.1024	0.2390	0.1191	0.1981	0.0039	0.0029	0.1541	0.0764	0.0916	0.0964
GC0073	0.2780	0.0956	0.0054	0.0071	0.0904	0.2333	0.2576	0.0903	0.2485	0.1609	0.1566	0.3139	0.1742	0.2773	0.0031	0.0037	0.2084	0.3216	0.2119	-
GC0077	0.0153	0.0142	0.0005	0.0007	0.0081	0.0135	0.0375	0.0102	0.0206	0.0117	0.0166	0.0234	0.0142	0.0199	0.0004	0.0004	0.0087	0.0319	0.0182	0.0083
GC0078	0.5700	0.3716	0.0079	0.0151	0.1657	0.3613	0.6064	0.1914	0.3476	0.2855	0.3042	0.3792	0.2263	0.4999	0.0043	0.0060	0.3640	0.1884	0.2527	-
GC0084	0.0577	0.0543	0.0026	0.0031	0.0446	0.0619	0.1418	0.0550	0.1058	0.0690	0.0811	0.1994	0.0942	0.1469	0.0019	0.0019	0.1492	0.1096	0.1989	0.1683
GC0086	0.0276	0.0155	0.0006	0.0007	0.0125	0.0415	0.0228	0.0125	0.0368	0.0234	0.0209	0.0701	0.0124	0.0638	0.0002	0.0004	0.0150	0.0130	0.0270	0.0100
GC0087	0.0211	0.0281	0.0010	0.0010	0.0107	0.0188	0.0260	0.0255	0.0491	0.0159	0.0223	0.0468	0.0152	0.0777	0.0004	0.0004	0.0162	0.0365	0.0290	0.0256
GC0088	0.2641	0.2721	0.0072	0.0084	0.1463	0.2113	0.2194	0.2148	0.4199	0.1854	0.2423	0.4010	0.1536	0.7722	0.0061	0.0067	0.3358	0.4639	0.2077	0.1977
GC0091	0.1023	0.0635	0.0031	0.0036	0.0616	0.1132	0.0938	0.0892	0.1545	0.0529	0.0916	0.2877	0.0697	0.1358	-	-	0.0803	-	-	-
GC0098	0.1802	0.1031	0.0063	0.0066	0.0890	0.2386	0.1831	0.1281	0.3717	0.1069	0.1514	0.4560	0.2250	0.4573	0.0061	0.0058	0.1941	0.2806	0.2108	0.1626
GC0105	0.7466	0.4718	0.0179	0.0255	0.4179	0.8374	1.5192	0.4483	0.9700	0.3916	0.6955	1.2085	0.5733	1.8883	0.0096	0.0131	0.5198	0.4582	0.7535	0.3713
GC0109	0.4218	0.2894	0.0107	0.0147	0.1583	0.2257	0.2522	0.1512	0.2928	0.1420	0.2411	0.4312	0.2696	0.3075	0.0041	0.0039	0.2265	0.2146	0.2957	-
GC0110	0.0274	0.0171	0.0007	0.0008	0.0132	0.0405	0.0321	0.0155	0.0391	0.0214	0.0474	0.0393	0.0302	0.0864	0.0009	0.0008	0.0281	0.0230	0.0175	0.0169
GC0116	0.2663	0.1554	0.0075	0.0090	0.1901	0.3292	0.4291	0.1801	0.5078	0.3158	0.5712	0.5262	0.2144	0.8919	0.0089	0.0078	0.4501	0.4543	0.2536	0.2924
GC0120	0.1489	0.0516	0.0022	0.0025	0.0441	0.0638	0.1189	0.0628	0.1225	0.0574	0.0608	0.1944	0.0672	0.1086	0.0027	0.0022	0.0610	0.0418	0.0502	0.0547
GC0121	0.0520	0.0336	0.0016	0.0020	0.0271	0.0792	0.0625	0.0341	0.1882	0.0337	0.0646	0.0916	0.0326	0.1492	-	-	0.0489	0.0634	-	-
GC0124	0.2191	0.1398	0.0043	0.0061	0.0591	0.0915	0.2297	0.0846	0.1430	0.0735	0.2123	0.2813	0.0870	0.3097	0.0020	0.0023	0.0818	0.1696	0.1383	0.0699
GC0127	0.3255	0.1348	0.0098	0.0119	0.1212	0.3043	0.3988	0.1371	0.3802	0.1078	0.2337	0.6748	0.1797	0.4783	0.0049	0.0052	0.1610	0.1820	0.2381	0.2161
GC0129	0.0154	0.0153	0.0005	0.0007	0.0082	0.0272	0.0235	0.0103	0.0264	0.0141	0.0180	0.0305	0.0143	0.0274	-	-	-	-	-	-
GC0130	0.1127	0.0728	0.0030	0.0036	0.0618	0.0931	0.2071	0.0936	0.2004	0.0634	0.0951	0.1781	0.0963	0.3408	-	-	0.0664	-	-	-
GC0132	0.1071	0.0741	0.0036	0.0043	0.0531	0.1482	0.2777	0.0661	0.1365	0.0606	0.1369	0.1032	0.0874	0.2999	0.0010	0.0012	0.0571	0.1277	0.0594	0.0700
GC0134	0.0120	0.0074	0.0003	0.0004	0.0051	0.0137	0.0147	0.0154	0.0145	0.0082	0.0169	0.0410	0.0088	0.0263	-	-	-	-	-	-
GC0137	0.1183	0.0636	0.0035	0.0033	0.0372	0.0604	0.0726	0.0401	0.0884	0.0650	0.0561	0.1689	0.0636	0.1905	0.0010	0.0017	0.0513	0.0872	0.1149	0.0593
GC0143	0.1083	0.0729	0.0052	0.0036	0.0778	0.1051	0.1491	0.0811	0.3419	0.1493	0.2263	0.4754	0.1170	0.4567	-	-	0.1097	0.2425	-	-
GC0145	0.0486	0.0221	0.0009	0.0011	0.0184	0.0323	0.0321	0.0198	0.0661	0.0306	0.0454	0.0832	0.0346	0.1412	0.0022	0.0013	0.0266	0.0313	0.0387	0.0344
GC0150	0.0490	0.0388	0.0010	0.0011	0.0311	0.0447	0.0910	0.0431	0.0372	0.0187	0.0420	0.0509	0.0282	0.0317	0.0008	0.0006	0.0211	0.0173	0.0217	0.0153
GC0154	0.3683	0.2441	0.0149	0.0160	0.2692	0.2889	0.4552	0.2893	0.4178	0.2355	0.3106	0.4520	0.2871	0.3535	0.0033	0.0045	0.2115	0.2369	0.3203	0.2619
GC0158	0.1775	0.1060	0.0050	0.0058	0.0848	0.1711	0.1337	0.1021	0.1508	0.0757	0.2314	0.1674	0.0584	0.2337	0.0016	0.0019	0.0820	0.0972	0.1285	0.0568
GC0161	0.2058	0.0834	0.0057	0.0050	0.0701	0.1877	0.1637	0.1013	0.5074	0.3222	0.1804	0.6423	0.2465	0.5155	0.0026	0.0033	0.2270	0.1301	0.1899	0.1920
GC0164	0.3595	0.1897	0.0062	0.0085	0.1386	0.3794	0.3921	0.1417	0.4002	0.1319	0.3215	0.3315	0.1488	0.3250	0.0034	0.0038	0.1289	0.1364	0.2024	0.1949
GC0165	0.1657	0.0722	0.0048	0.0052	0.0804	0.2286	0.1015	0.0808	0.3396	0.0798	0.1086	0.1598	0.1116	0.3601	0.0014	0.0018	0.0578	0.1162	0.1371	0.0728
GC0186	0.2286	0.3084	0.0056	0.0092	0.2142	0.4272	0.3194	0.2022	0.2916	0.2352	0.1880	0.4337	0.1804	0.3332	0.0030	0.0034	0.1718	0.3000	0.2804	0.1849
GC0188	0.3133	0.0859	0.0052	0.0079	0.0819	0.2258	0.2262	0.1307	0.3206	0.2137	0.5464	0.5433	0.1287	0.6155	0.0061	0.0056	0.1421	0.2130	0.2912	0.1506
GC0193	0.2206	0.1665	0.0108	0.0084	0.1389	0.1873	0.1993	0.1132	0.8463	0.4863	0.7995	0.9850	0.3636	0.5006	0.0116	0.0145	0.2275	0.3203	0.5411	0.4847
GC0197	0.1793	0.1083	0.0098	0.0099	0.0789	0.1613	0.1666	0.0959	0.2589	0.1061	0.3853	0.5928	0.2139	0.3065	0.0025	0.0031	0.1925	0.1951	0.1846	0.1254
GC0199	0.0776	0.0495	0.0022	0.0042	0.0756	0.1142	0.0768	0.0721	0.1222	0.0835	0.1252	0.3218	0.0798	0.1667	0.0028	0.0026	0.1932	0.2086	0.2103	0.0795
GC0205	0.1684	0.0726	0.0034	0.0030	0.0469	0.0777	0.0637	0.0576	0.0759	0.0690	0.1056	0.2546	0.0490	0.2396	0.0032	0.0027	0.0560	0.0453	0.1308	0.0615
GC0208	0.0692	0.0280	0.0016	0.0022	0.0314	0.0423	0.0578	0.0276	0.0663	0.0480	0.0823	0.1012	0.0325	0.0814	0.0015	0.0021	0.0522	0.0561	0.0494	0.0525
GC0210	0.1679	0.0965	0.0046	0.0060	0.0719	0.1365	0.1932	0.0828	0.1842	0.0866	0.1858	0.3313	0.0956	0.4112	0.0023	0.0032	0.1017	0.1173	0.1303	0.1315
GC0211	0.1208	0.0820	0.0073	0.0094	0.1106	0.1074	0.1125	0.1803	0.2316	0.0782	0.1472	0.2347	0.1225	0.1628	0.0013	0.0017	0.0568	0.0668	0.1364	-
GC0215	0.1003	0.0283	0.0027	0.0031	0.0370	0.0522	0.0418	0.0289	0.0612	0.0380	0.0414	0.0488	0.0260	0.0637	-	-	0.0442	0.0353	-	-
GC0226	0.4789	0.2717	0.0151	0.0159	0.1407	0.3281														

TABLE 5 — *Continued*

GC Name	H δ_A (Å)	H δ_F (Å)	CN ₁ (mag)	CN ₂ (mag)	Ca4227 (Å)	G4300 (Å)	H γ_A (Å)	H γ_F (Å)	Fe4383 (Å)	Ca4455 (Å)	Fe4531 (Å)	C4668 (Å)	H β (Å)	Fe5015 (Å)	Mg ₁ (mag)	Mg ₂ (mag)	Mg _b (Å)	Fe5270 (Å)	Fe5335 (Å)	Fe5406 (Å)
GC0233	0.5367	0.4637	0.0136	0.0166	0.1883	0.4677	0.3431	0.2931	0.4094	0.1924	0.3479	0.4224	0.1975	0.8439	-	-	-	-	-	-
GC0238	0.2076	0.0923	0.0024	0.0046	0.0497	0.1350	0.1249	0.0505	0.1820	0.0982	0.1585	0.0780	0.0787	0.3740	-	-	-	-	-	-
GC0239	0.0798	0.0949	0.0042	0.0050	0.0479	0.1283	0.1583	0.0606	0.1438	0.0581	0.1233	0.2170	0.0777	0.2824	0.0022	0.0039	0.0813	0.1111	0.1123	0.0937
GC0243	0.7767	0.8046	0.0233	0.0335	0.4015	1.0093	1.1668	0.4697	0.8297	0.3020	1.0291	1.2363	0.9590	1.2857	-	-	0.5908	-	-	-
GC0245	0.0458	0.0444	0.0024	0.0030	0.0278	0.0383	0.0835	0.0337	0.0608	0.0464	0.0936	0.0926	0.0388	0.1249	0.0010	0.0011	0.0524	0.0530	0.0485	0.0416
GC0248	0.2807	0.1581	0.0126	0.0116	0.1113	0.2368	0.1581	0.1111	0.3689	0.1115	0.2998	0.2629	0.1053	0.3674	-	-	0.1485	-	-	-
GC0249	0.2068	0.0965	0.0044	0.0050	0.1169	0.1320	0.2640	0.1031	0.2873	0.0876	0.1872	0.2484	0.1828	0.4632	0.0047	0.0041	0.1481	0.1546	0.2815	0.1587
GC0255	0.8397	0.5932	0.0186	0.0231	0.3078	0.4710	1.0389	0.3820	1.0393	0.3082	0.4496	0.5852	0.3797	0.7800	0.0062	0.0073	0.2076	0.2080	0.2478	-
GC0265	0.0254	0.0141	0.0006	0.0009	0.0111	0.0209	0.0479	0.0147	0.0322	0.0145	0.0314	0.0734	0.0167	0.0556	0.0004	0.0004	0.0415	0.0170	0.0319	0.0184
GC0266	0.1146	0.0563	0.0021	0.0027	0.0342	0.0448	0.0570	0.0392	0.0870	0.0342	0.1187	0.1777	0.0347	0.1115	0.0008	0.0009	0.0381	0.0571	0.0374	0.0380
GC0272	1.3574	0.4577	0.0184	0.0204	0.3250	0.8300	1.0878	0.3810	1.4102	0.3495	0.7339	1.1316	0.2800	1.2366	0.0058	0.0068	0.3739	0.3361	0.4588	0.2733
GC0273	0.5843	0.3022	0.0086	0.0219	0.1427	0.2807	0.3388	0.2020	0.4992	0.1342	0.2668	0.5109	0.1189	0.2473	-	-	-	-	-	-
GC0277	0.0645	0.0313	0.0011	0.0015	0.0262	0.0399	0.0444	0.0323	0.0686	0.0292	0.0498	0.0963	0.0354	0.0717	0.0017	0.0023	0.0444	0.0453	0.0385	0.0424
GC0278	0.1933	0.1419	0.0053	0.0064	0.0540	0.0707	0.1750	0.1520	0.1055	0.0440	0.1058	0.1584	0.0397	0.0825	-	-	0.0499	-	-	-
GC0279	1.9630	0.6320	0.0248	0.0286	0.3884	1.0114	0.9142	0.4494	1.3610	0.3500	1.0546	1.2675	0.8695	1.0794	0.0110	0.0122	0.4657	1.0181	0.5415	0.5589
GC0281	0.1600	0.1028	0.0067	0.0105	0.0840	0.1282	0.1522	0.0864	0.1767	0.0701	0.2312	0.2098	0.0946	0.2960	-	-	0.0786	-	-	-
GC0282	0.1559	0.1242	0.0061	0.0069	0.1015	0.1207	0.2182	0.0738	0.1350	0.0859	0.1014	0.2578	0.0699	0.2165	0.0027	0.0025	0.0639	0.0625	0.0785	0.0616
GC0286	0.1287	0.0426	0.0033	0.0031	0.0312	0.0422	0.0569	0.0524	0.0891	0.0538	0.0513	0.2045	0.0735	0.1413	0.0012	0.0012	0.0799	0.0799	0.0455	0.0450
GC0289	0.0467	0.0379	0.0016	0.0016	0.0240	0.0332	0.0376	0.0490	0.0499	0.0408	0.0556	0.1123	0.0342	0.0783	0.0008	0.0009	0.0716	0.0579	0.0367	0.0539
GC0291	0.1218	0.0815	0.0037	0.0074	0.0716	0.2460	0.1288	0.2021	0.1968	0.1237	0.2702	0.2760	0.1031	0.1876	0.0019	0.0019	0.0742	0.1857	0.1038	0.0959
GC0292	0.9144	0.5588	0.0239	0.0280	0.4679	0.5682	0.7951	0.7553	1.5398	0.4501	0.5145	1.3143	0.4686	1.1155	0.0048	0.0070	0.2437	0.4206	0.3488	0.2822
GC0295	0.3609	0.3586	0.0156	0.0175	0.1296	0.3668	0.2357	0.1815	0.8099	0.1872	0.2466	1.0504	0.1778	0.2565	0.0026	0.0030	0.1585	0.1067	0.2239	0.1270
GC0299	0.6344	0.4592	0.0229	0.0323	0.3619	0.8768	0.7116	0.3395	0.7120	0.3451	0.5314	0.8060	0.4331	1.1804	0.0072	0.0075	0.2760	0.3317	0.5556	0.3345
GC0300	0.3710	0.1872	0.0041	0.0046	0.1495	0.1606	0.1590	0.0855	0.2319	0.1478	0.1705	0.2315	0.0869	0.5309	0.0079	0.0077	0.1300	0.1893	0.1169	0.0728
GC0303	0.2360	0.0748	0.0048	0.0061	0.0762	0.1353	0.0740	0.0786	0.1045	0.0478	0.1246	0.2068	0.0947	0.1110	0.0008	0.0012	0.0834	0.0930	0.0638	0.0429
GC0312	0.6873	0.5359	0.0204	0.0458	1.9185	0.5897	1.3996	0.3899	1.1873	1.5113	0.5282	0.9577	0.2947	1.1475	0.0076	0.0079	0.4440	0.3899	0.6058	0.3203
GC0313	0.2186	0.1149	0.0139	0.0132	0.1565	0.3362	0.3020	0.1872	0.4213	0.2560	0.2929	0.7812	0.2046	0.6019	0.0056	0.0062	0.2644	0.2857	0.2890	0.2915
GC0314	0.1807	0.0665	0.0044	0.0061	0.0690	0.1102	0.1387	0.0573	0.2925	0.0923	0.1177	0.3150	0.0875	0.2223	0.0040	0.0057	0.1377	0.2021	0.6251	0.1311
GC0316	0.5823	0.1441	0.0066	0.0069	0.1267	0.2095	0.2063	0.1254	0.2823	0.1156	0.2151	0.3116	0.2069	0.2860	0.0029	0.0031	0.1376	0.2168	0.2413	0.1379
GC0317	0.1589	0.1197	0.0061	0.0064	0.0830	0.1806	0.1310	0.0939	0.1615	0.1332	0.2721	0.4607	0.1370	0.2741	0.0029	0.0029	0.1136	0.2244	0.3737	-
GC0319	0.1202	0.1290	0.0032	0.0041	0.0816	0.1498	0.1098	0.0924	0.1339	0.0631	0.2060	0.4447	0.0857	0.2177	0.0032	0.0040	0.1106	0.1274	0.2017	-
GC0321	0.2309	0.1374	0.0146	0.0063	0.1201	0.1616	0.3364	0.1956	0.2358	0.1749	0.3010	0.3491	0.1451	0.3582	-	-	0.1260	0.1687	-	-
GC0325	1.0192	0.3539	0.0144	0.0185	0.2741	0.6976	0.4792	0.3635	0.8423	0.2584	0.3458	0.5818	0.2242	0.5353	0.0048	0.0060	0.4446	0.3229	0.2839	0.2623
GC0326	0.0342	0.0341	0.0012	0.0011	0.0192	0.0567	0.0756	0.0185	0.0579	0.0188	0.0323	0.0628	0.0214	0.0613	-	-	0.0369	-	-	-
GC0328	0.2563	0.3086	0.0090	0.0107	0.2564	0.5960	0.5172	0.2011	0.4279	0.1805	0.3513	0.4318	0.1620	0.5253	0.0097	0.0121	0.2014	0.2578	0.3330	0.1877
GC0330	0.0229	0.0208	0.0006	0.0008	0.0124	0.0191	0.0196	0.0101	0.0209	0.0162	0.0154	0.0564	0.0122	0.0237	-	-	0.0234	-	-	-
GC0331	0.0915	0.0747	0.0045	0.0039	0.0444	0.0864	0.0947	0.0478	0.1552	0.0878	0.0615	0.1556	0.0543	0.1671	0.0018	0.0026	0.0607	0.0824	0.0885	0.0657
GC0340	0.4459	0.3128	0.0203	0.0232	0.2367	0.3747	0.4334	0.2321	0.4698	0.1834	0.4712	0.7623	0.1844	0.4348	0.0058	0.0066	0.1772	0.1649	0.4677	0.2372
GC0365	0.0254	0.0106	0.0006	0.0004	0.0058	0.0109	0.0141	0.0071	0.0246	0.0108	0.0250	0.0301	0.0090	0.0356	0.0004	0.0004	0.0109	0.0155	0.0104	0.0085
GC0367	0.0853	0.0527	0.0027	0.0025	0.0372	0.0583	0.0630	0.0706	0.0972	0.0660	0.1610	0.1419	0.0668	0.2355	0.0016	0.0017	0.1316	0.2407	0.1003	0.0616
GC0370	0.0775	0.0569	0.0021	0.0031	0.0388	0.1132	0.0719	0.0419	0.0769	0.0497	0.0803	0.1795	0.0931	0.1284	0.0013	0.0017	0.1143	0.0811	0.1020	0.0548
GC0420	0.1652	0.0559	0.0033	0.0046	0.0775	0.0827	0.0916	0.0627	0.1220	0.0796	0.1036	0.4667	0.0721	0.1566	0.0035	0.0039	0.1572	0.2225	0.1303	0.0935
GC0424	0.0453	0.0312	0.0015	0.0019	0.0281	0.0629	0.0471	0.0329	0.1701	0.0712	0.0652	0.1218	0.0911	0.0852	-	-	0.0907	-	-	-
GC0425	0.2837	0.2093	0.0084	0.0092	0.1811	0.2766	0.3012	0.2303	0.6062	0.4006	0.5826	0.7344	0.3385	0.8105	0.0080	0.0084	0.2577	0.2959	0.4840	0.2941
GC0426	0.4526	0.1522	0.0061	0.0060	0.1556	0.1898	0.3666	0.1550	0.2005	0.1698	0.2080	0.3146	0.2361	0.4742	0.0088	0.0093	0.2562	0.3243	0.4737	0.2005
GC0436	0.1138	0.0757	0.0037	0.0046	0.0720	0.1385	0.2809	0.1363	0.3592	0.0654	0.1885	0.1576	0.0458	0.1203	-	-	0.0689	-	-	-
GC0445	0.1423	0.1035	0.0035	0.0036	0.0490	0.1842	0.1255	0.0748	0.3763	0.1789	0.1784	0.2898	0.1540	0.4041	0.0056	0.0067	0.1023	0.0939	0.1580	0.1121
GC0446	0.4259	0.1774	0.0059	0.0069	0.1120	0.2108	0.3490	0.1539	0.2487	0.0931	0.1548	0.3403	0.1068	0.3349	0.0032	0.0034	0.1761	0.2556	0.1224	0.0811
GC0447	0.4252	0.1967	0.0101	0.0142	0.2225	0.7744	0.4605	0.1939	0.5145	0.2891	0.3852	1.9313	0.3116	0.5716	0.0186	0.0167	0.7026	0.3381	0.5507	0.4887
GC0448	0.3516	0.1262	0.0114	0.0098	0.0837	0.2302	0.3710	0.1092	0.7655	0.0890	0.1561	0.8096	0.2329	0.4586	0.0026	0.0030	0.1156	0.1208	0.2290	0.0938
GC0449	0.2533	0.0908	0.0032	0.0040	0.0558	0.1053	0.1121	0.0679	0.1380	0.0957	0.0971	0.1532	0.0707	0.5028	0.0020	0.0016	0.1395	0.0570	0.0825	0.0606
GC0450	0.1873	0.0609	0.0024	0.0025	0.0508	0.1732	0.0789	0.1312	0.1357	0.1022	0.2123	0.2291	0.1667	0.2076	0.0023	0.0029	0.0929	0.1668	0.1024	0.0742
GC0451	0.4614	0.4680	0.0125	0.0148	0.2460	0.4026	0.5476	0.33												

TABLE 5 — *Continued*

GC Name	H δ_A (Å)	H δ_F (Å)	CN ₁ (mag)	CN ₂ (mag)	Ca4227 (Å)	G4300 (Å)	H γ_A (Å)	H γ_F (Å)	Fe4383 (Å)	Ca4455 (Å)	Fe4531 (Å)	C ₄ 668 (Å)	H β (Å)	Fe5015 (Å)	Mg ₁ (mag)	Mg ₂ (mag)	Mg _b (Å)	Fe5270 (Å)	Fe5335 (Å)	Fe5406 (Å)
GC0455	0.2156	0.0772	0.0037	0.0042	0.0854	0.1026	0.2438	0.0751	0.1741	0.1008	0.2307	0.2092	0.0909	0.4177	-	-	0.0717	0.2678	-	-
GC0456	0.1164	0.0336	0.0015	0.0018	0.0424	0.0595	0.0435	0.0329	0.0647	0.0339	0.0546	0.0771	0.0393	0.0918	0.0012	0.0014	0.0425	0.0655	0.0676	0.0716
GC0457	1.3989	0.7069	0.0234	0.0324	0.3754	0.7178	0.7910	0.4754	1.1399	0.7153	0.7247	1.1431	0.4838	1.3077	0.0140	0.0148	0.7438	0.4465	0.4222	0.4840
GC0458	0.5122	0.2761	0.0061	0.0106	0.1083	0.1980	0.1672	0.1292	0.3065	0.1393	0.5648	0.9233	0.3386	0.4783	0.0051	0.0063	0.3591	0.6221	0.3138	0.4827
GC0459	0.6744	0.8158	0.0203	0.0271	1.3314	0.8124	3.5247	0.6668	1.0890	0.6559	0.7186	1.7876	0.7063	2.8577	0.0135	0.0149	0.5574	0.8546	1.1738	0.4529
GC0460	0.3042	0.1649	0.0057	0.0117	0.0899	0.4479	0.5319	0.3931	0.6001	0.1526	0.2029	0.0988	0.1728	0.3982	0.0094	0.0119	0.1445	0.2108	0.3659	0.1521
GC0461	0.3785	0.1216	0.0089	0.0138	0.0991	0.1606	0.3089	0.1736	0.3378	0.2126	0.3152	0.5123	0.3928	1.1215	0.0044	0.0059	0.2315	0.1897	0.3063	0.2966
GC0462	0.0258	0.0187	0.0012	0.0021	0.0143	0.0711	0.0275	0.0185	0.0400	0.0358	0.0508	0.1908	0.0411	0.0859	0.0008	0.0009	0.0381	0.0522	0.0449	0.0365
GC0463	0.2358	0.1649	0.0084	0.0078	0.1116	0.1508	0.1325	0.1133	0.4990	0.0863	0.3053	0.2548	0.0940	0.4594	0.0030	0.0040	0.0722	0.1206	0.1543	0.1119
GC0464	0.5667	0.4988	0.0450	0.0157	0.2643	0.4996	0.5011	0.9165	0.8670	0.7742	0.6861	0.8994	0.4857	0.5670	0.0212	0.0111	0.5228	0.4912	0.5646	0.2551
GC0465	0.5314	0.3771	0.0126	0.0126	0.1888	1.0286	1.0200	0.2164	0.4193	0.4108	0.8058	0.5538	0.2870	0.8146	0.0073	0.0087	0.7882	0.8609	0.4807	0.3430
GC0466	0.2170	0.0984	0.0043	0.0063	0.0886	0.2114	0.1536	0.1231	0.2120	0.1463	0.1652	0.2748	0.1832	0.4259	0.0036	0.0044	0.3433	0.4545	0.2489	0.1732
GC0467	1.3158	1.1062	0.0331	0.0438	0.3687	0.9742	1.7218	0.5913	2.0400	0.5737	1.2651	1.7621	0.5127	1.4383	0.0337	0.0380	1.1807	0.5885	0.9900	0.5822
GC0467	0.1336	0.0847	0.0104	0.0109	0.0785	0.2120	0.1567	0.1137	0.2104	0.1879	0.1597	0.3385	0.0747	0.1784	-	-	0.1058	-	-	-
GC0469	0.5153	0.3900	0.0186	0.0237	0.2497	0.3705	0.7868	0.3462	0.7983	0.2901	0.5724	1.3487	0.5167	1.4179	0.0092	0.0114	0.3528	0.4817	0.4511	0.5255
GC0470	1.4648	0.5928	0.0379	0.0529	0.4322	0.6513	0.6866	0.3367	0.7596	0.5383	0.5880	0.8911	0.3391	0.8493	-	-	-	-	-	-
GC0471	0.1749	0.1289	0.0059	0.0077	0.1024	0.2839	0.5123	0.1307	0.8004	0.2398	0.2258	0.6034	0.1548	0.3986	-	-	0.3667	-	-	-
GC0472	0.6055	0.2466	0.0189	0.0189	0.1709	0.2972	0.2819	0.2267	0.7191	0.3346	0.3983	1.1401	0.3356	0.7478	0.0079	0.0089	0.3160	0.3762	0.6942	0.3740
GC0473	0.3618	0.2852	0.0155	0.0135	0.3316	0.5591	0.4739	0.2682	0.7052	0.5719	0.4972	0.6467	0.3136	0.5684	-	-	0.5933	-	-	-
GC0474	0.2863	0.1600	0.0107	0.0144	0.1701	0.3055	0.2406	0.1323	0.5446	0.4226	0.3498	0.5826	0.3779	0.3734	0.0037	0.0045	0.1664	0.1836	0.6053	-
GC0475	2.1342	1.5649	0.0836	0.0834	0.9664	0.9813	2.8506	1.1567	1.1854	0.7950	1.8065	2.4944	0.5967	1.3275	0.0229	0.0251	1.0733	0.7728	1.3733	0.6581
GC0476	0.1819	0.1221	0.0032	0.0041	0.1040	0.2297	0.1304	0.0813	0.3340	0.1250	0.1389	0.2319	0.0830	0.2124	0.0026	0.0022	0.0861	0.0865	0.1072	0.1399
GC0477	1.1993	1.0140	0.0417	0.0436	0.6882	1.0020	2.7621	1.6713	1.3193	0.9903	1.2518	2.0438	1.1579	3.2121	0.0196	0.0216	0.7737	2.1101	0.8761	0.7212
GC0478	0.0982	0.0692	0.0030	0.0034	0.0505	0.1822	0.1067	0.0593	0.1412	0.0895	0.2062	0.1692	0.0825	0.1741	0.0013	0.0014	0.1320	0.0772	0.0651	0.0519
GC0479	1.0693	0.2435	0.0185	0.0180	0.3261	0.3041	0.3966	0.2503	0.6299	0.4702	0.5957	1.2883	0.3391	0.7891	0.0078	0.0084	0.7810	0.3906	0.5188	0.4600

Spectroscopy of Globular Clusters in NGC 5128

TABLE 6
 AGES, METALLICITIES, AND $[\alpha/\text{Fe}]$ OF GLOBULAR CLUSTERS IN NGC
 5128

GC Name	Age (Gyr)	[Z/H] (dex)	$[\alpha/\text{Fe}]$ (dex)
GC0046	$8.4^{+3.4}_{-0.3}$	$-1.05^{+0.06}_{-0.15}$	$-0.10^{+0.03}_{-0.02}$
GC0049	$10.8^{+4.1}_{-4.2}$	$-0.89^{+0.16}_{-0.24}$	$0.14^{+0.13}_{-0.12}$
GC0050	$6.8^{+5.1}_{-4.4}$	$-0.29^{+0.56}_{-0.20}$	$-0.99^{+0.17}_{-0.01}$
GC0052 ^a	$11.5^{+2.2}_{-2.4}$	$-1.67^{+0.16}_{-0.10}$	$0.02^{+0.29}_{-0.27}$
GC0057 ^b	$12.0^{+1.2}_{-3.1}$	$-1.04^{+0.19}_{-0.14}$	$-0.11^{+0.08}_{-0.08}$
GC0062	$11.3^{+0.6}_{-1.0}$	$-1.22^{+0.14}_{-0.03}$	$0.15^{+0.24}_{-0.22}$
GC0065	$9.3^{+3.9}_{-2.2}$	$-1.01^{+0.16}_{-0.24}$	$0.01^{+0.19}_{-0.18}$
GC0068	$10.5^{+0.7}_{-2.0}$	$-0.56^{+0.05}_{-0.02}$	$0.40^{+0.09}_{-0.09}$
GC0070	$9.3^{+2.7}_{-0.6}$	$-1.12^{+0.12}_{-0.12}$	$0.15^{+0.03}_{-0.03}$
GC0073	$4.8^{+6.0}_{-2.5}$	$-0.70^{+0.60}_{-0.54}$	$-0.99^{+0.04}_{-0.01}$
GC0077	$12.3^{+0.1}_{-0.1}$	$-0.12^{+0.01}_{-0.01}$	$0.40^{+0.01}_{-0.01}$
GC0078	$4.3^{+0.6}_{-1.3}$	$0.14^{+0.07}_{-0.14}$	$-0.99^{+0.02}_{-0.01}$
GC0084	$6.2^{+0.4}_{-0.4}$	$-2.05^{+0.19}_{-0.13}$	$0.16^{+0.25}_{-0.24}$
GC0086	$9.3^{+0.1}_{-0.2}$	$0.08^{+0.01}_{-0.01}$	$0.07^{+0.01}_{-0.01}$
GC0087	$11.3^{+0.1}_{-0.1}$	$-1.01^{+0.01}_{-0.01}$	$0.27^{+0.01}_{-0.01}$
GC0088	$9.9^{+4.3}_{-1.0}$	$-0.36^{+0.08}_{-0.11}$	$0.41^{+0.10}_{-0.08}$
GC0098	$12.6^{+1.2}_{-0.8}$	$-0.33^{+0.02}_{-0.02}$	$0.65^{+0.07}_{-0.06}$
GC0109	$8.8^{+1.2}_{-2.4}$	$-0.62^{+0.09}_{-0.07}$	$-0.99^{+0.08}_{-0.01}$
GC0110	$9.2^{+0.2}_{-0.2}$	$0.45^{+0.01}_{-0.01}$	$0.63^{+0.01}_{-0.01}$
GC0120	$4.2^{+0.4}_{-0.3}$	$-0.12^{+0.02}_{-0.02}$	$-0.06^{+0.01}_{-0.01}$
GC0124	$12.0^{+1.1}_{-0.9}$	$-0.43^{+0.02}_{-0.02}$	$0.35^{+0.04}_{-0.02}$
GC0127	$4.9^{+1.7}_{-0.9}$	$-0.27^{+0.05}_{-0.06}$	$0.17^{+0.06}_{-0.06}$
GC0132	$3.8^{+0.4}_{-0.4}$	$0.14^{+0.12}_{-0.02}$	$-0.02^{+0.01}_{-0.02}$
GC0145	$10.3^{+0.2}_{-2.6}$	$-0.46^{+0.04}_{-0.01}$	$0.17^{+0.01}_{-0.01}$
GC0150	$2.1^{+0.1}_{-0.1}$	$0.10^{+0.01}_{-0.01}$	$-0.99^{+0.01}_{-0.01}$
GC0158	$10.2^{+0.2}_{-0.1}$	$0.06^{+0.02}_{-0.02}$	$0.13^{+0.02}_{-0.02}$
GC0165	$7.5^{+0.2}_{-0.2}$	$-0.60^{+0.02}_{-0.02}$	$-0.06^{+0.05}_{-0.04}$
GC0188	$3.0^{+0.4}_{-0.3}$	$-0.39^{+0.07}_{-0.04}$	$0.21^{+0.10}_{-0.09}$
GC0197	$10.9^{+1.4}_{-1.4}$	$-1.40^{+0.07}_{-0.15}$	$-0.07^{+0.13}_{-0.13}$
GC0199	$5.2^{+2.9}_{-0.7}$	$-1.04^{+0.16}_{-0.23}$	$-0.44^{+0.16}_{-0.15}$
GC0208	$3.8^{+0.1}_{-0.2}$	$-0.44^{+0.01}_{-0.01}$	$-0.01^{+0.02}_{-0.02}$
GC0230	$4.6^{+0.4}_{-0.3}$	$-0.08^{+0.02}_{-0.02}$	$0.20^{+0.03}_{-0.02}$
GC0239	$11.4^{+0.5}_{-1.4}$	$-1.27^{+0.05}_{-0.02}$	$-0.15^{+0.06}_{-0.07}$
GC0245	$10.9^{+0.1}_{-0.2}$	$-1.39^{+0.01}_{-0.01}$	$-0.26^{+0.03}_{-0.03}$
GC0249	$7.8^{+0.9}_{-1.1}$	$-0.18^{+0.06}_{-0.04}$	$-0.08^{+0.05}_{-0.05}$
GC0265	$8.6^{+0.1}_{-0.1}$	$-0.61^{+0.01}_{-0.01}$	$0.08^{+0.01}_{-0.01}$
GC0266	$6.6^{+0.3}_{-0.1}$	$-0.39^{+0.01}_{-0.01}$	$0.34^{+0.02}_{-0.01}$
GC0272	$11.4^{+2.3}_{-3.0}$	$-1.74^{+0.31}_{-0.24}$	$0.12^{+0.25}_{-0.24}$
GC0277	$6.2^{+2.6}_{-0.3}$	$-0.36^{+0.01}_{-0.04}$	$-0.07^{+0.02}_{-0.02}$
GC0279	$9.6^{+3.3}_{-3.5}$	$-0.96^{+0.27}_{-0.33}$	$0.37^{+0.37}_{-0.33}$
GC0282	$8.7^{+0.8}_{-0.5}$	$-0.53^{+0.01}_{-0.02}$	$0.25^{+0.02}_{-0.02}$
GC0286	$11.3^{+0.3}_{-0.1}$	$-0.59^{+0.01}_{-0.01}$	$0.30^{+0.02}_{-0.01}$
GC0289 ^c	$10.6^{+0.3}_{-0.1}$	$-1.41^{+0.01}_{-0.01}$	$0.16^{+0.03}_{-0.04}$
GC0291	$12.1^{+0.1}_{-0.2}$	$-1.25^{+0.08}_{-0.06}$	$0.40^{+0.17}_{-0.18}$
GC0292	$11.6^{+1.9}_{-1.9}$	$-0.45^{+0.04}_{-0.04}$	$0.57^{+0.11}_{-0.09}$
GC0299	$9.0^{+4.1}_{-2.3}$	$-0.50^{+0.07}_{-0.11}$	$0.26^{+0.14}_{-0.13}$
GC0300	$9.7^{+2.3}_{-0.7}$	$-0.88^{+0.07}_{-0.08}$	$0.35^{+0.07}_{-0.06}$
GC0303	$4.7^{+0.7}_{-0.8}$	$0.06^{+0.03}_{-0.02}$	$0.17^{+0.01}_{-0.02}$
GC0312	$12.0^{+2.1}_{-3.5}$	$-0.54^{+0.10}_{-0.09}$	$-0.01^{+0.15}_{-0.14}$
GC0313	$10.3^{+2.0}_{-1.8}$	$-1.56^{+0.15}_{-0.12}$	$-0.09^{+0.21}_{-0.20}$
GC0314	$6.3^{+5.3}_{-2.2}$	$-0.31^{+0.67}_{-0.42}$	$0.99^{+0.01}_{-1.13}$
GC0317	$9.0^{+4.2}_{-5.9}$	$-1.35^{+1.17}_{-0.25}$	$-0.99^{+0.04}_{-0.04}$
GC0319	$8.5^{+4.0}_{-3.8}$	$-0.73^{+0.85}_{-0.24}$	$0.99^{+0.01}_{-0.06}$
GC0325	$8.8^{+3.6}_{-1.4}$	$-0.54^{+0.08}_{-0.14}$	$0.47^{+0.08}_{-0.08}$
GC0328	$8.0^{+3.3}_{-1.1}$	$-0.71^{+0.06}_{-0.10}$	$0.27^{+0.08}_{-0.07}$
GC0331	$5.6^{+0.5}_{-0.3}$	$-0.02^{+0.02}_{-0.03}$	$0.02^{+0.02}_{-0.02}$

TABLE 6
AGES, METALLICITIES, AND $[\alpha/\text{Fe}]$ OF GLOBULAR CLUSTERS IN NGC 5128

GC0340	$9.6^{+0.6}_{-3.4}$	$-0.64^{+0.09}_{-0.05}$	$0.11^{+0.15}_{-0.15}$
GC0365	$4.6^{+0.1}_{-0.1}$	$-0.32^{+0.01}_{-0.01}$	$0.01^{+0.01}_{-0.01}$
GC0367	$11.7^{+0.1}_{-0.4}$	$-1.38^{+0.03}_{-0.01}$	$0.99^{+0.01}_{-0.08}$
GC0370	$11.8^{+2.1}_{-0.6}$	$-0.37^{+0.02}_{-0.02}$	$0.15^{+0.02}_{-0.02}$
GC0425	$8.6^{+3.3}_{-1.0}$	$-1.08^{+0.22}_{-0.12}$	$0.45^{+0.19}_{-0.18}$
GC0426	$10.6^{+2.3}_{-1.3}$	$-1.09^{+0.19}_{-0.14}$	$0.99^{+0.29}_{-0.29}$
GC0446	$4.9^{+0.9}_{-0.9}$	$0.24^{+0.08}_{-0.06}$	$0.35^{+0.02}_{-0.02}$
GC0451 ^d	$10.9^{+2.1}_{-2.5}$	$-1.41^{+0.29}_{-0.09}$	$0.03^{+0.27}_{-0.30}$
GC0453	$5.7^{+0.1}_{-0.1}$	$0.30^{+0.01}_{-0.01}$	$0.11^{+0.01}_{-0.01}$
GC0456	$12.4^{+0.1}_{-3.0}$	$-1.18^{+0.12}_{-0.04}$	$-0.00^{+0.04}_{-0.04}$
GC0457	$8.8^{+2.2}_{-3.8}$	$0.04^{+0.28}_{-0.18}$	$0.02^{+0.09}_{-0.08}$
GC0460	$8.2^{+0.2}_{-0.1}$	$-0.91^{+0.02}_{-0.02}$	$-0.99^{+0.05}_{-0.01}$
GC0462	$10.5^{+1.2}_{-0.1}$	$-1.03^{+0.03}_{-0.02}$	$-0.14^{+0.04}_{-0.03}$
GC0472	$3.5^{+3.7}_{-0.9}$	$-0.46^{+0.09}_{-0.14}$	$0.19^{+0.21}_{-0.17}$
GC0476	$11.4^{+0.3}_{-0.4}$	$-1.70^{+0.03}_{-0.01}$	$0.52^{+0.09}_{-0.09}$
GC0478	$10.9^{+0.9}_{-0.7}$	$-1.23^{+0.04}_{-0.01}$	$0.24^{+0.04}_{-0.04}$

- ^a From a second spectrum with lower S/N we found age= $9.2^{+0.1}_{-0.1}$ Gyr, $[\text{Z}/\text{H}] = -1.51^{+0.01}_{-0.01}$ and $[\alpha/\text{Fe}] = -0.23^{+0.06}_{-0.06}$.
^b From a second spectrum with lower S/N we found age= $8.8^{+0.1}_{-0.9}$ Gyr, $[\text{Z}/\text{H}] = -0.78^{+0.03}_{-0.01}$ and $[\alpha/\text{Fe}] = 0.11^{+0.02}_{-0.03}$.
^c From a second spectrum with lower S/N we found age= $8.2^{+1.1}_{-0.2}$ Gyr, $[\text{Z}/\text{H}] = -1.43^{+0.03}_{-0.02}$ and $[\alpha/\text{Fe}] = -0.62^{+0.05}_{-0.05}$.
^d From a second spectrum with lower S/N we found age= $9.3^{+3.9}_{-4.8}$ Gyr, $[\text{Z}/\text{H}] = -1.08^{+0.92}_{-0.09}$ and $[\alpha/\text{Fe}] = -0.50^{+0.06}_{-0.07}$.

TABLE 7
RMIX FITS FOR FIGURE 10

Distribution	Modality	NGC 5128					Milky Way				
		Proportion	Mean	Sigma	χ_{red}^2	p-value	Proportion	Mean	Sigma	χ_{red}^2	p-value
Age	unimodal	1.0	8.58±0.33	2.78±0.23	2.40	0.003	1.0	11.33±0.23	1.50±0.17	2.22	0.018
	bimodal	0.29±0.07	4.85±0.47	1.32±0.35	1.12	0.346	0.52±0.18	11.19±0.47	2.03±0.42	0.89	0.522
		0.71±0.07	10.12±0.28	1.44±0.22			0.48±0.18	11.47±0.20	0.38±0.16		
	trimodal	0.32±0.07	5.02±0.46	1.41±0.36	0.74	0.617	-	-	-		
		0.25±0.09	8.76±0.26	0.56±0.26			-	-	-		
0.43±0.08		11.11±0.24	0.75±0.02			-	-	-			
Metallicity	unimodal	1.0	-0.68±0.07	0.55±0.05	1.29	0.200	1.0	-0.95±0.08	0.53±0.06	1.28	0.197
	bimodal	0.37±0.10	-1.27±0.11	0.29±0.08	1.43	0.158	0.58±0.09	-1.35±0.07	0.28±0.06	1.13	0.343
		0.63±0.10	-0.35±0.09	0.34±0.06			0.42±0.09	-0.40±0.06	0.19±0.05		
	trimodal	0.35±0.11	-1.25±0.07	0.28±0.05	1.41	0.218	0.35±0.09	-1.55±0.05	0.14±0.04	2.10	0.123
		0.44±0.11	-0.48±0.05	0.14±0.11			0.23±0.09	-1.04±0.46	0.07±0.70		
[α /Fe]	unimodal	0.21±0.10	0.09±0.11	0.15±0.07			0.43±0.08	-0.40±0.06	0.19±0.05		
		1.0	0.16±0.28	0.21±0.02	0.59	0.824	1.0	0.31±0.03	0.20±0.02	1.27	0.250
		0.72±0.37	0.07±0.10	0.15±0.05	0.79	0.558	-	-	-		
		0.28±0.37	0.40±0.20	0.15±0.08			-	-	-		

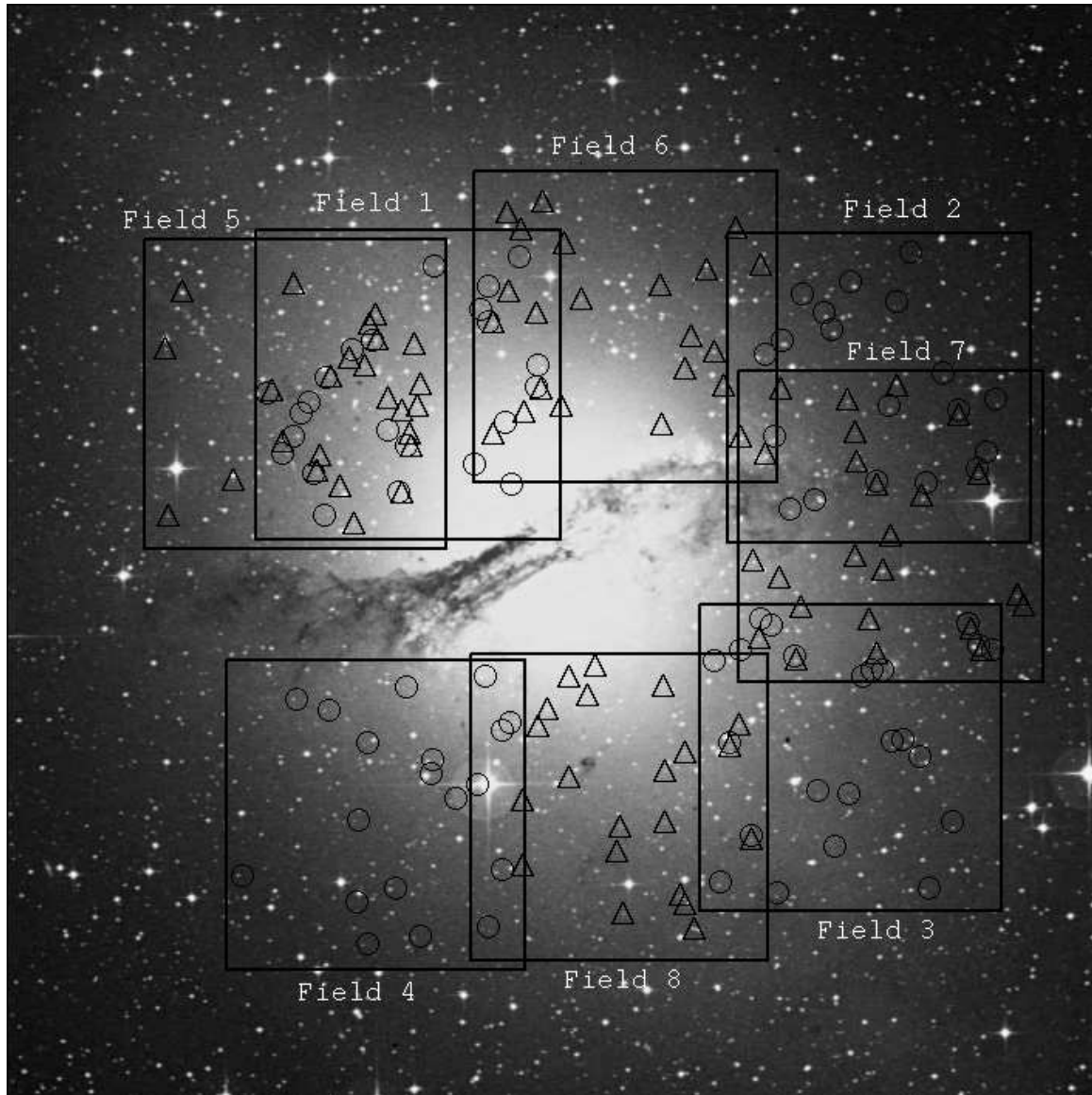


FIG. 1.— The positions of GMOS fields 1-4 GMOS from 2005 and fields 5-8 from 2007. The squares indicate a $5.5'$ region and the circles (triangles) indicate where the observed objects are located in each field from 2005 (2007). The fields are overplotted on a DSS image of NGC 5128, clearly showing the field's proximity to the center of the galaxy.

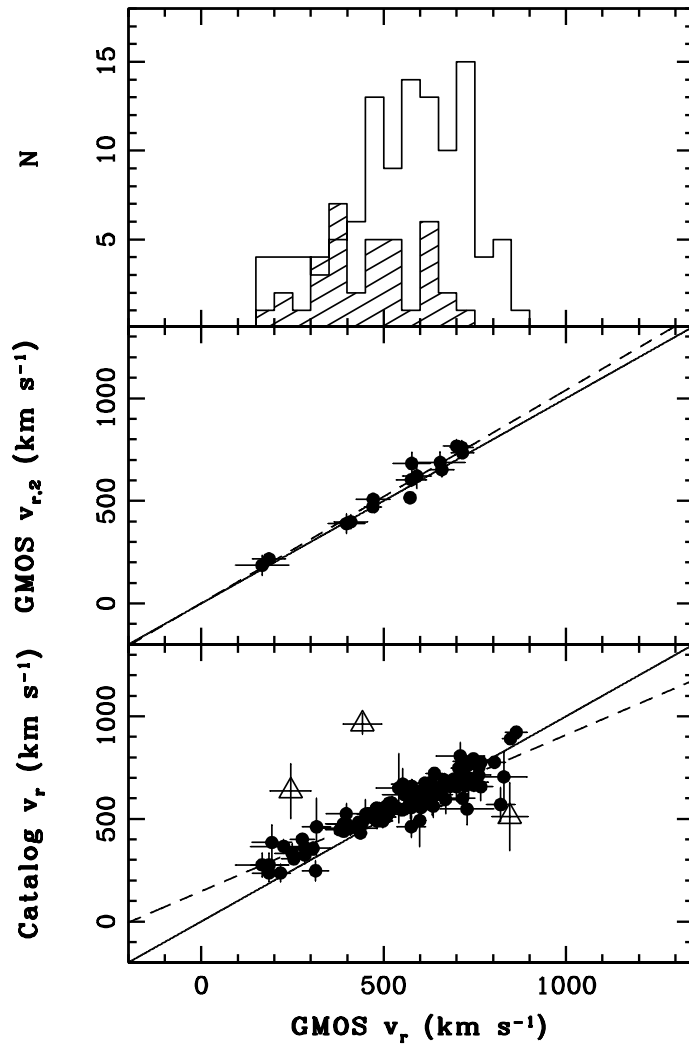


FIG. 2.— *Top*: The projected radial velocities measured with Gemini/GMOS for the previously known GCs in Table 2 (open histogram) and the newly discovered GCs in Table 3 (hatched histogram). *Middle*: A comparison of radial velocities of GCs measured twice with GMOS. The lines are a 1:1 (solid) and a least square fit with slope = 1.04 and y-intercept = 1.071 with an rms error of 34 km s^{-1} about the line. *Bottom*: The radial velocity of the GCs measured with GMOS compared to the cataloged velocity from Woodley et al. (2007) and from M. Gómez & K. A. Woodley (2009, in preparation). The lines are a 1:1 (solid) and a least squares fit with slope = 0.76 and y-intercept = 147.5 with and rms error of 72 km s^{-1} about the line. The open triangles are GC0049 (measured once before from Peng et al. (2004b)) and GC0188 and GC0226 (both measured once before in Beasley et al. (2008), removed from the fit).

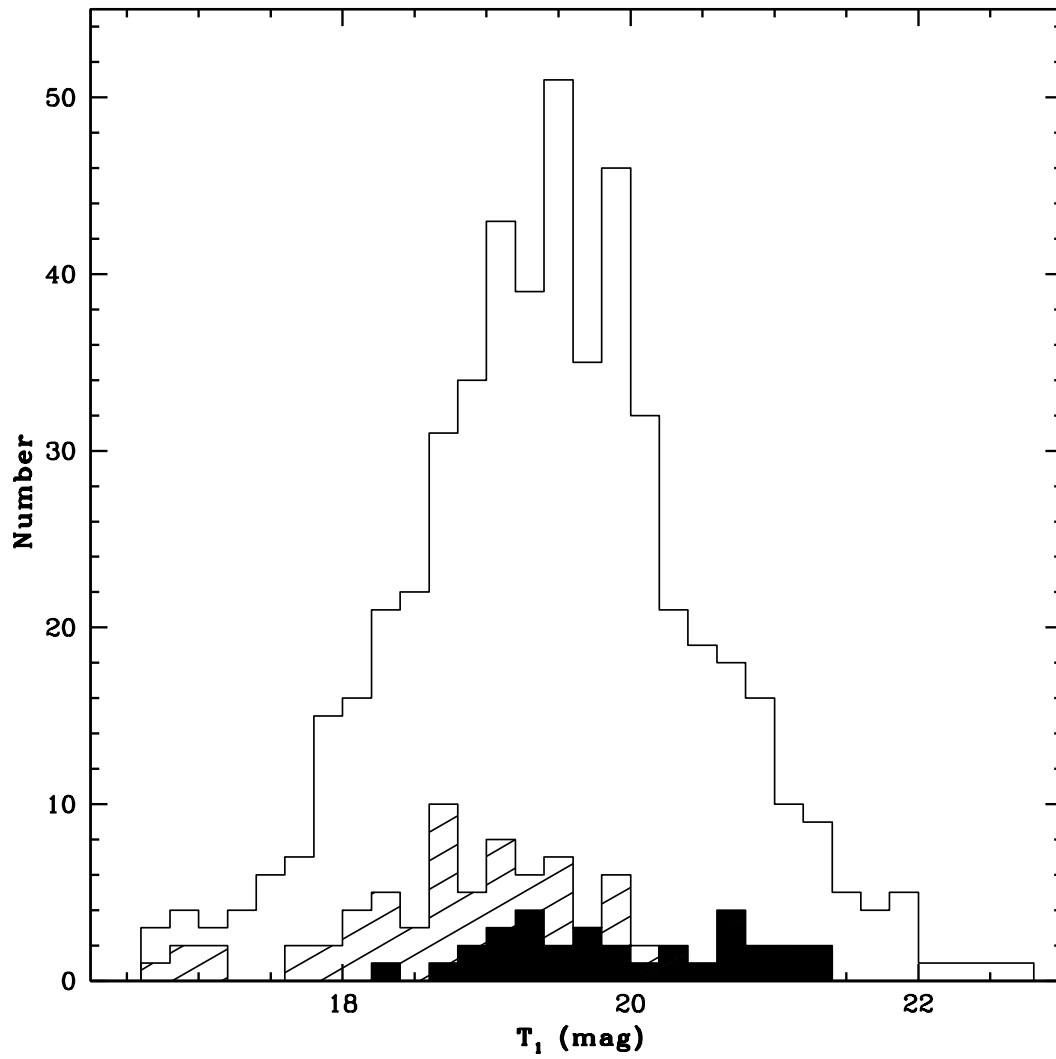


FIG. 3.— The luminosity functions for the entire GCS of NGC 5128, consisting of 524 GCs with T_1 measurements (*open histogram*), 33 of the newly confirmed GCs from this study that have T_1 magnitudes (*solid histogram*), and 69 of the targetted 72 GCs with available T_1 magnitudes with ages, metallicities, and $[\alpha/\text{Fe}]$ from this study (*hatched histogram*).

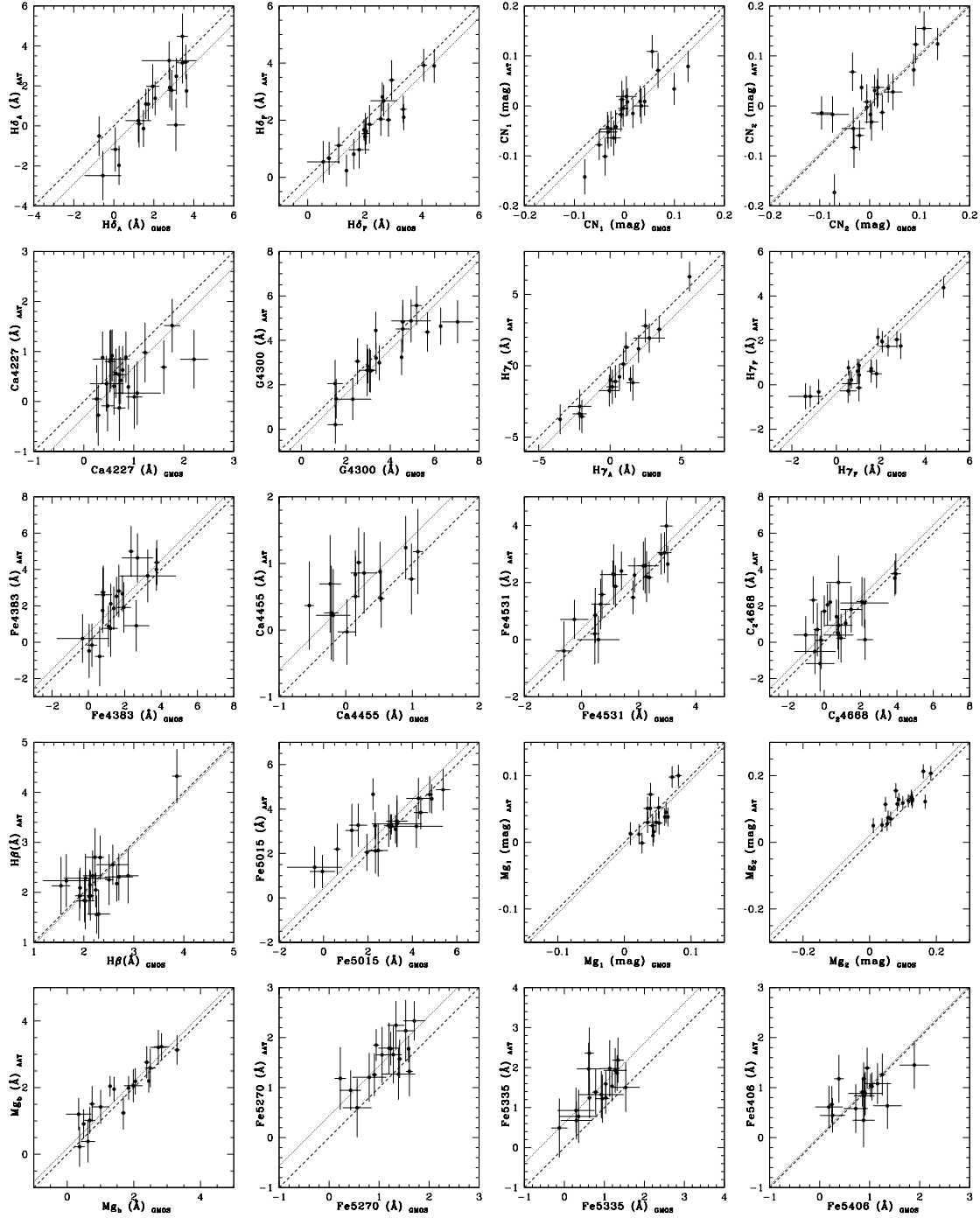


FIG. 4.— The calibration of index measurement from the common GMOS spectra of 2005 with those of the AAT study by Beasley et al. (2008), which have been calibrated to the Lick index system. All globular clusters within 2σ of the mean shift between the two systems were kept for the fit. The dashed line is the one-to-one line and the dotted line is the mean shift with a slope of one. Within the scatter of the two datasets, the mean shift is a valid correction to the Lick index system.

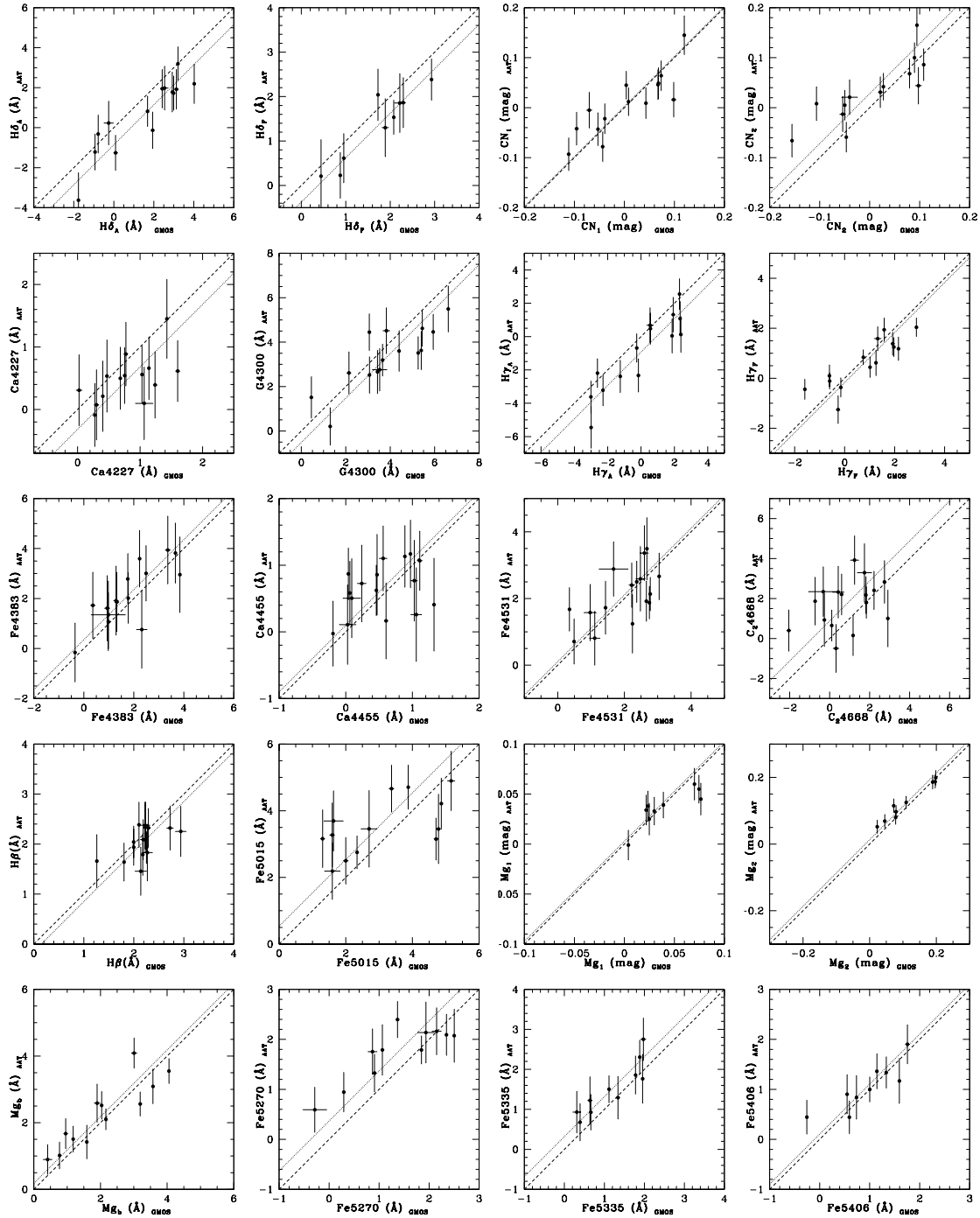


FIG. 5.— The same as Figure 4 but for the calibration of the GMOS 2007 dataset to the AAT study by Beasley et al. (2008).

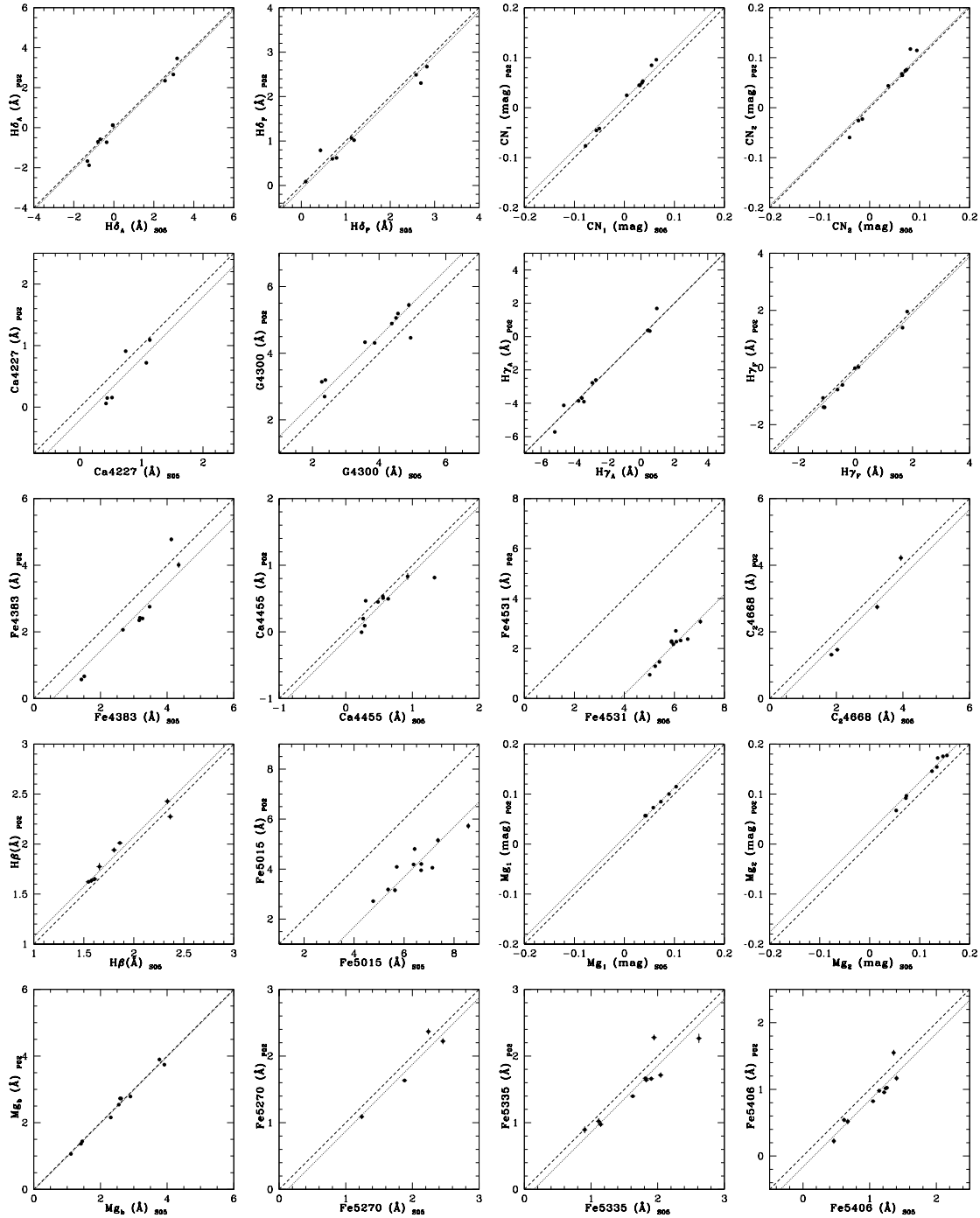


FIG. 6.— The same as Figure 4 but for the calibration of the Schiavon et al. (2005) dataset to the Puzia et al. (2002) dataset for the Milky Way GCs. The indices Fe4383 and Fe5015 were not used for any comparisons or calculations because of their unreliable index measurements caused by defects in the Schiavon et al. (2005) spectra.

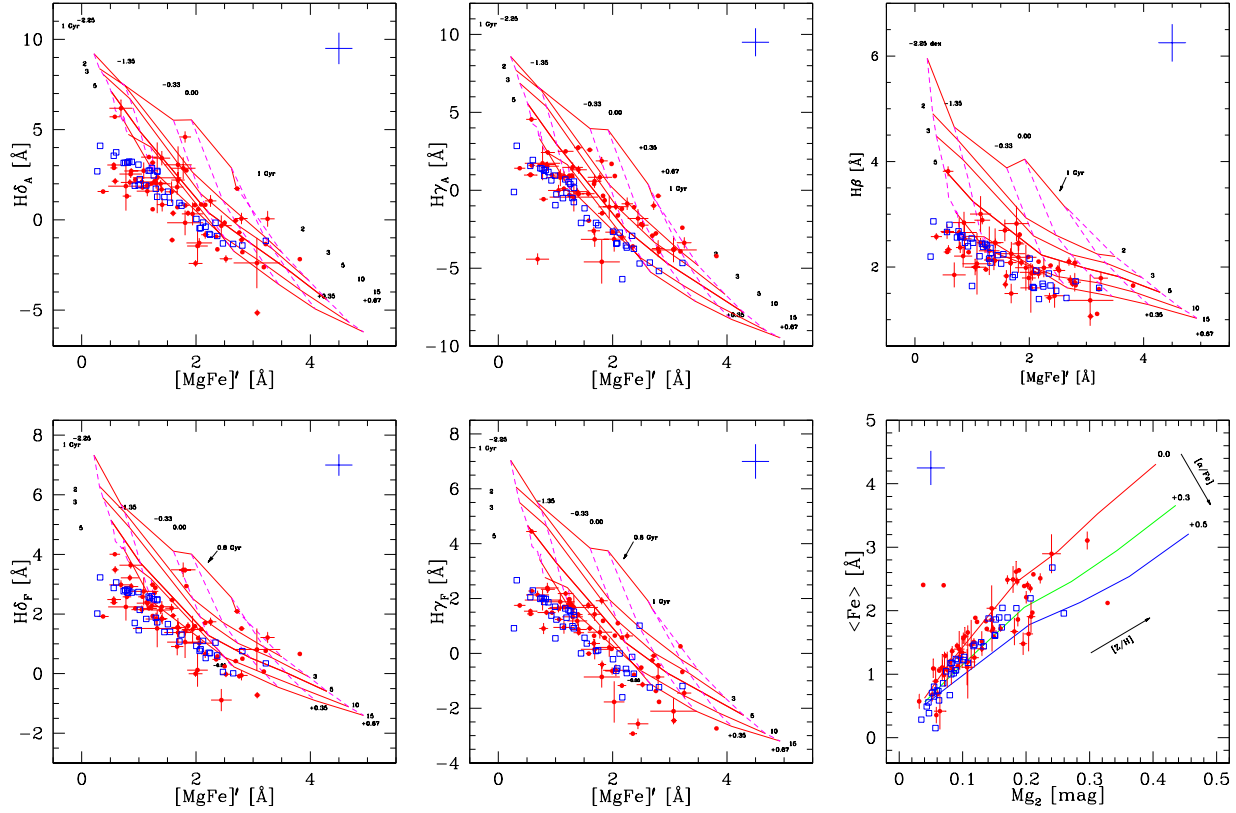


FIG. 7.— Diagnostic plots for all measurements (no duplicate measurements) of GCs in NGC 5128 with $S/N > 30\text{\AA}^{-1}$ (*red circles*) and the Milky Way data (Schiavon et al. 2005; Puzia et al. 2002) (*blue squares*). The SSP models are from Thomas et al. (2003, 2004) and the Balmer line diagnostic plots are for the grids of $[\alpha/\text{Fe}] = 0.0$ dex. The bootstrapping uncertainty is attached to each point and the systematic uncertainty is indicated by the *blue cross* in the corner.

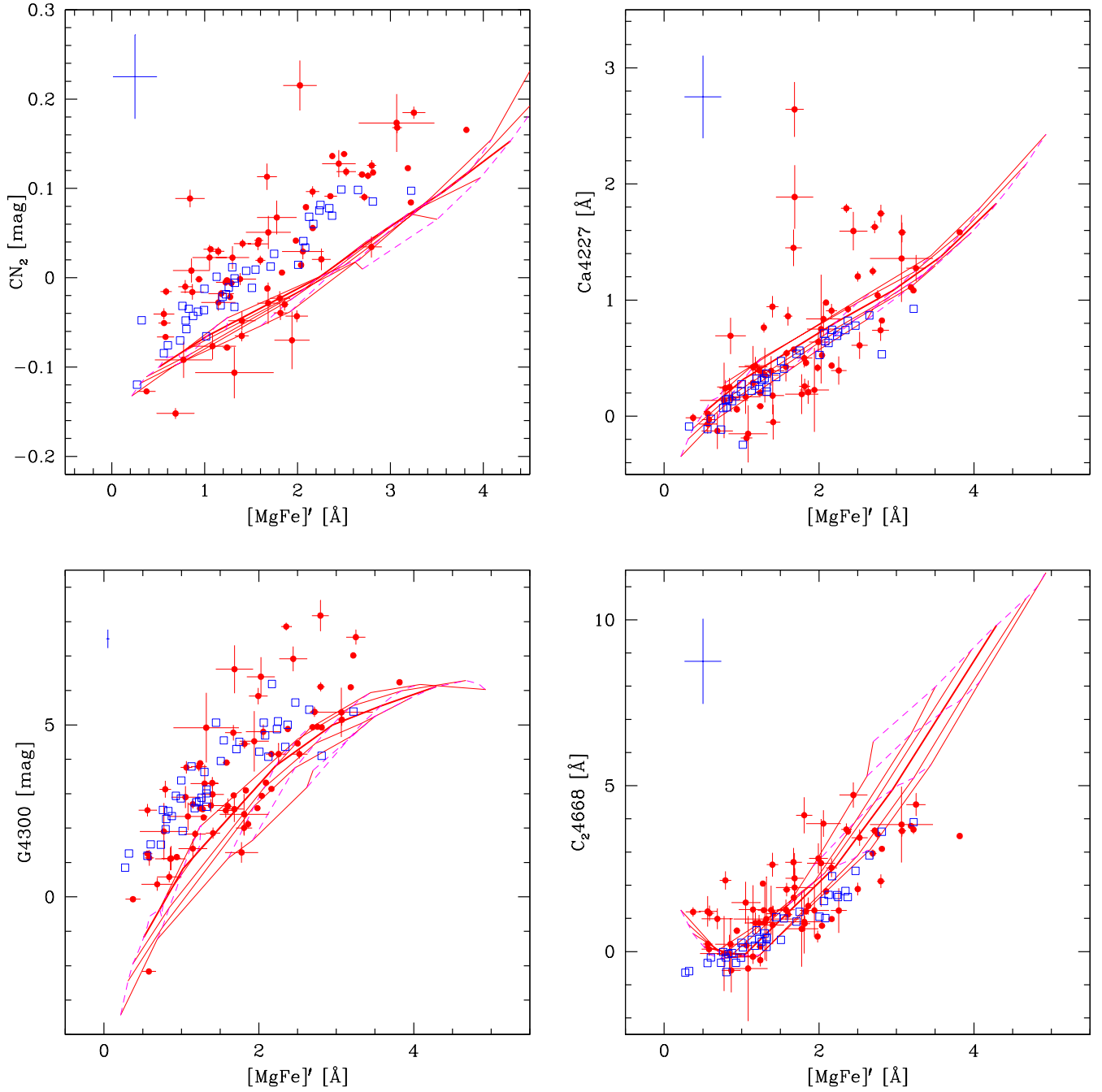


FIG. 8.— Diagnostic plots for calcium, carbon, and nitrogen sensitive elements of GCs in NGC 5128 with $S/N > 30 \text{Å}^{-1}$ (*red circles*) and the Milky Way data (Schiavon et al. 2005; Puzia et al. 2002) (*blue squares*). The SSP models are from Thomas et al. (2003, 2004) and the Balmer line diagnostic plots are for the grids of $[\alpha/Fe] = 0.0$ dex. The bootstrapping uncertainty is attached to each point and the systematic uncertainty is indicated by the *blue cross* in the corner.

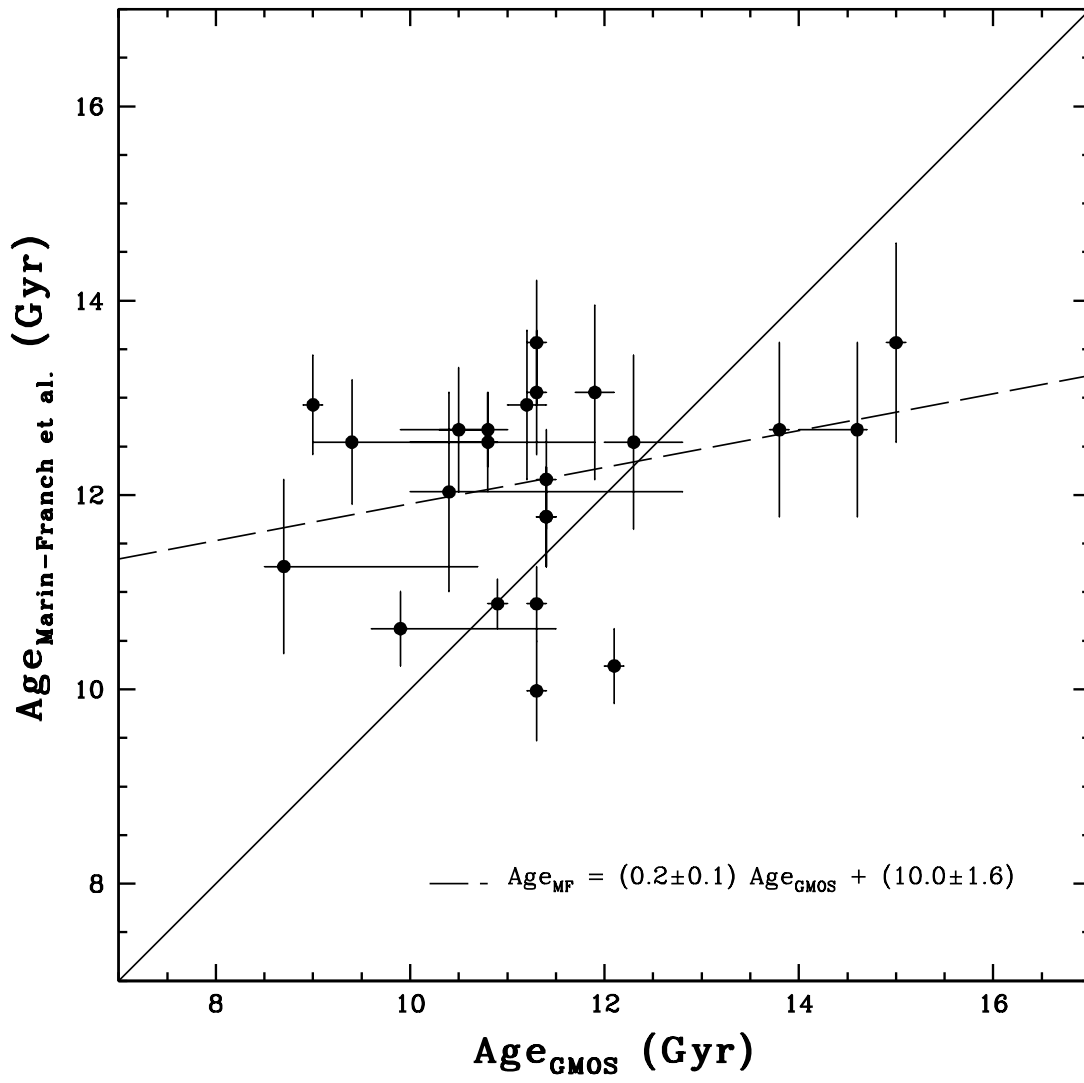


FIG. 9.— A comparison of the ages of 24 Milky Way GCs in common between this study and that of relative age main sequence fitting of Marin-Franch et al. (2008). A 1:1 *solid line* is shown as well as the least squared fit (*dashed line*) with a slope and intercept of 0.2 ± 0.1 and 10.0 ± 1.6 and an rms= 0.97.

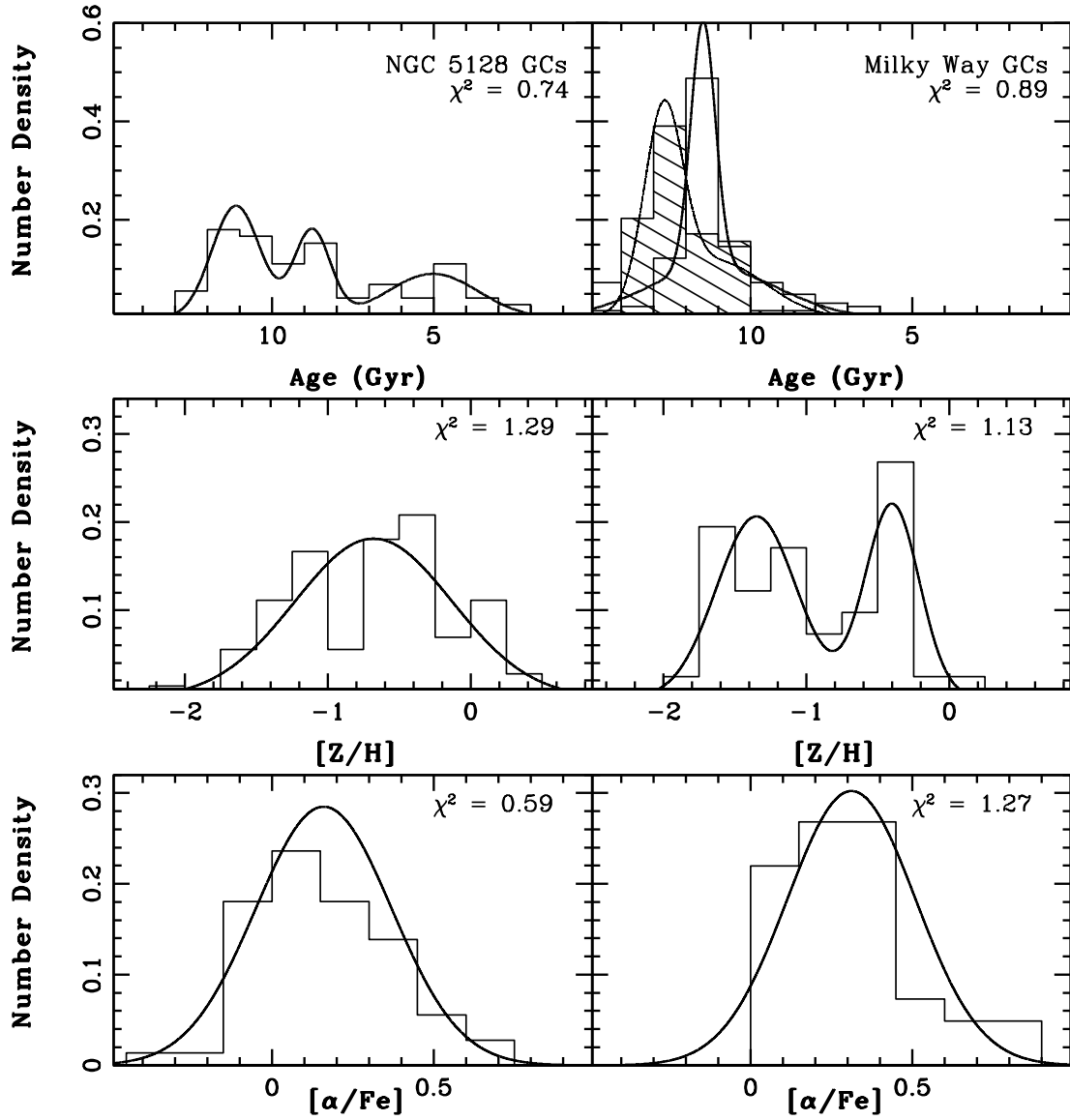


FIG. 10.— The age (*top panels*), metallicity (*middle panels*), and $[\alpha/\text{Fe}]$ (*bottom panels*) distribution functions for 72 GCs in NGC 5128 (*left*) and for 41 Milky Way GCs (*right*) derived from the SSP models of Thomas et al. (2003) with varying α -elemental abundance (Thomas et al. 2004). The summed best fit Gaussian distributions are overplotted (*solid line*), with reduced χ^2 values indicated. The fits are listed in Table 7. The cross-hatched histogram in the Milky Way age distribution is the result from Marín-Franch et al. (2008), with best fit bimodal distribution (*dot dashed line*) of $(0.44 \pm 0.09, 11.07 \pm 0.63, 1.52 \pm 0.25)$ and $(0.56 \pm 0.09, 12.71 \pm 0.20, 0.59 \pm 0.22)$ with reduced $\chi^2 = 0.21$.

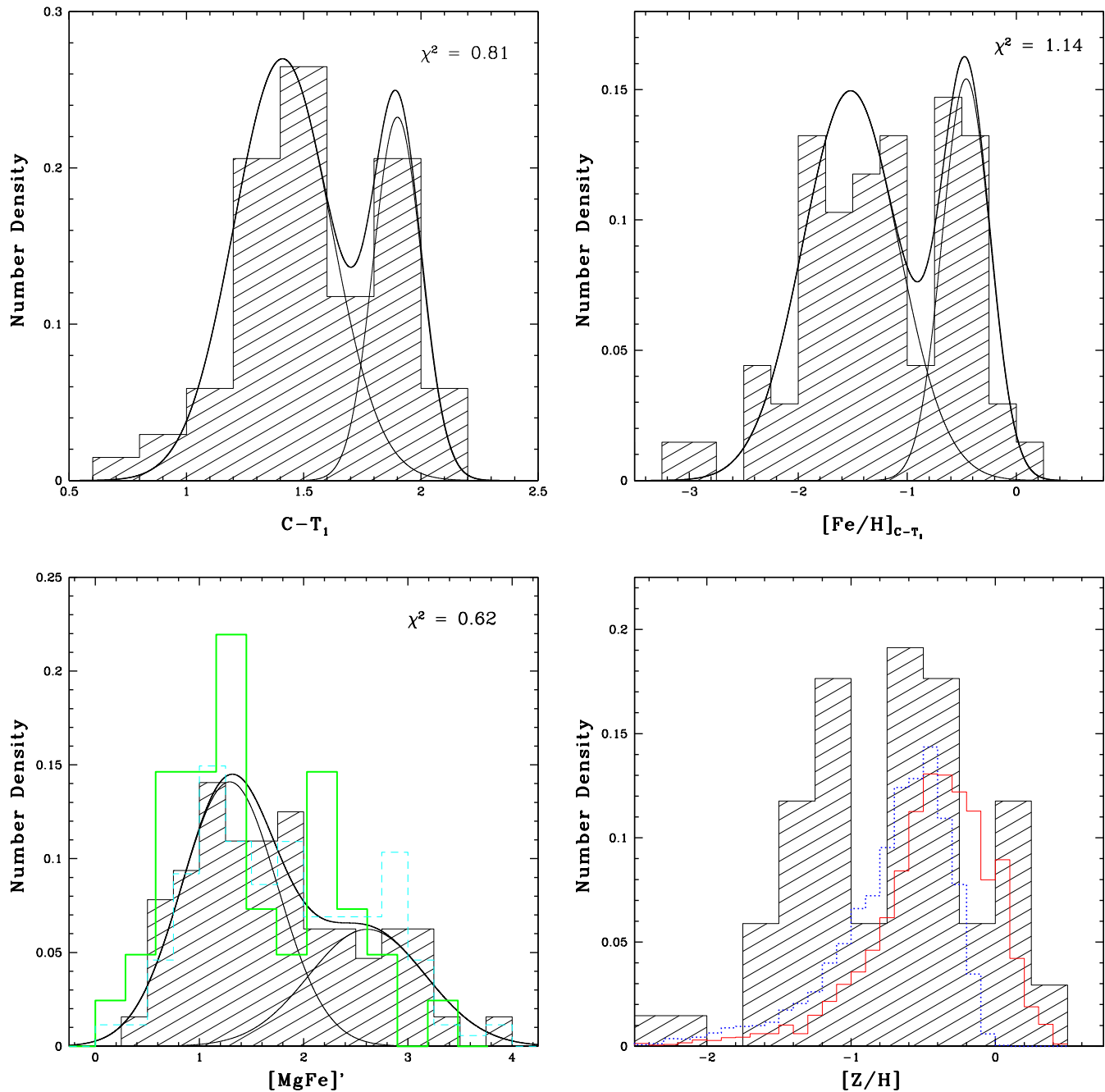


FIG. 11.— Various distributions of 68 GCs in NGC 5128 with determined metallicity and available $(C-T_1)$ from Harris et al. (2004), with the best fit Gaussian distributions and their summation overplotted. *Top left:* The color distribution, $(C-T_1)$, with best fit Gaussian distributions. The fitted parameters are (proportion of total sample, peak, sigma) = $(0.70 \pm 0.08, 1.41 \pm 0.04, 0.21 \pm 0.04)$ and $(0.30 \pm 0.08, 1.90 \pm 0.04, 0.10 \pm 0.26)$, with a $\chi^2_{red} = 0.81$. *Top right:* The metallicity, $[Fe/H]_{c-t_1}$ transformed from the color index, $(C-T_1)$ (see text). The fitted parameters are $(0.66 \pm 0.08, -1.52 \pm 0.10, 0.44 \pm 0.08)$ and $(0.34 \pm 0.08, -0.46 \pm 0.07, 0.22 \pm 0.05)$, with a $\chi^2_{red} = 1.14$. *Bottom left:* The distribution of the metallicity $[MgFe]'$ index derived from our measured spectroscopy. The fitted parameters for a bimodal distribution are $(0.65 \pm 0.33, 1.29 \pm 0.29, 0.46 \pm 0.15)$ and $(0.35 \pm 0.33, 2.61 \pm 0.73, 0.56 \pm 0.35)$, with a $\chi^2_{red} = 0.62$. A unimodal distribution has a $\chi^2_{red} = 1.02$. The *open thick green histogram* is for the 41 Milky Way GCs used in this study (Schiavon et al. 2005; Puzia et al. 2002). The *hatched blue histogram* is for the combination of all available NGC 5128 data from this study with $S/N > 30\text{\AA}$ and from Beasley et al. (2008). No duplicate GCs are used in this plot, totalling 174 GCs. *Bottom right:* The metallicity obtained from the SSP models (Thomas et al. 2003, 2004). The best fit distributions are shown in Fig. 10. Overplotted are the distributions of the stellar halo in NGC 5128 for the inner halo, 8 kpc (*red open histogram*) and the combination of two outer fields at 21 and 31 kpc (*dashed blue histogram*) (Harris & Harris 2000, 2002; Rejkuba et al. 2005).

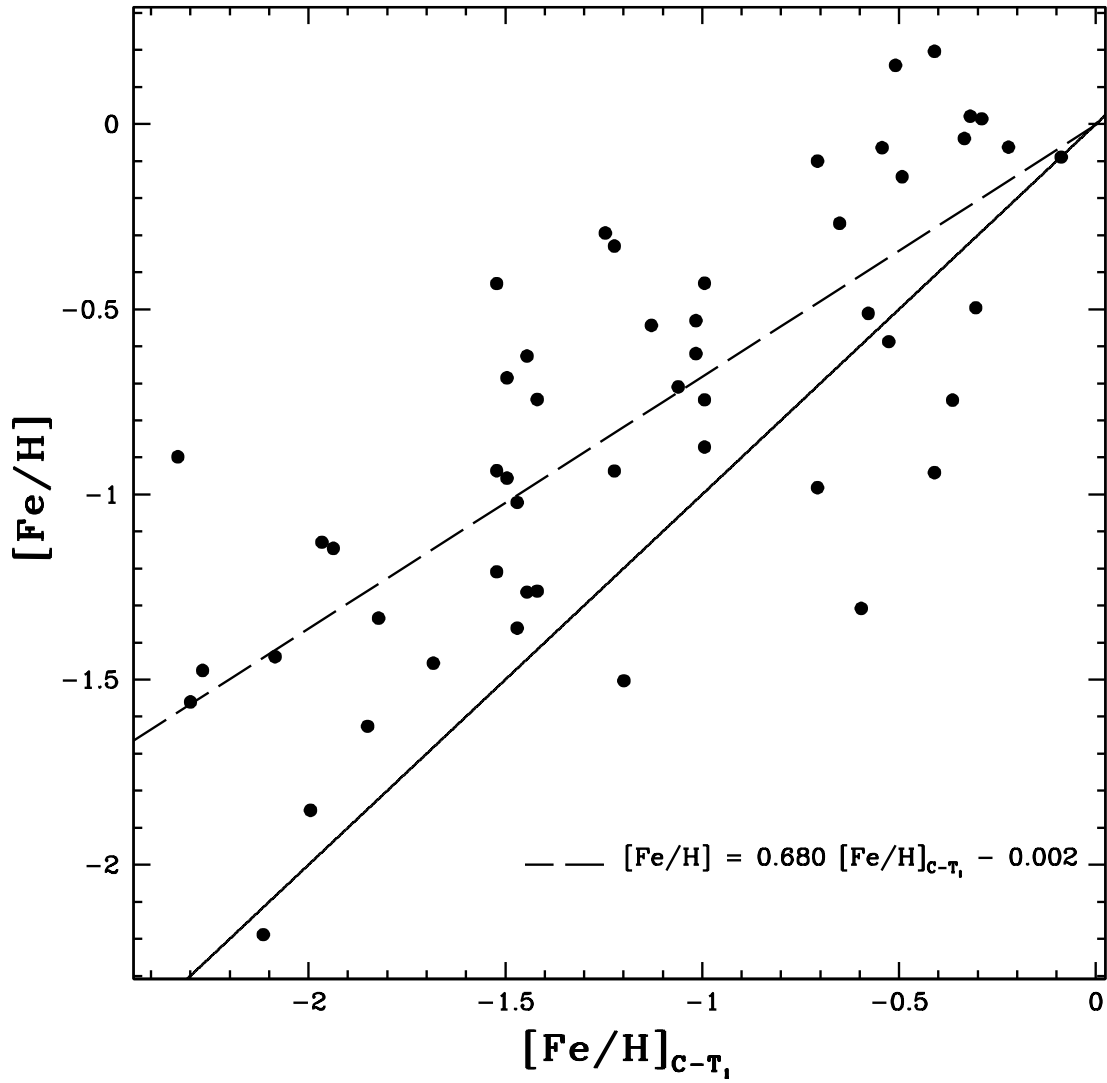


FIG. 12.— Metallicity, $[Fe/H]_{C-T_1}$, derived from the color (C-T₁) compared to the SSP model determined $[Fe/H]$ value for the GCs in NGC 5128. The 1:1 line is shown as a *solid line*. The best fit line is shown as a *dashed line* after 5 points were removed based on the Chauvenet Criteria (Parratt 1961). It appears there is not a direct one-to-one correlation either due to potential non-linearity in the color-to-metallicity conversion or due to the model interpolation.

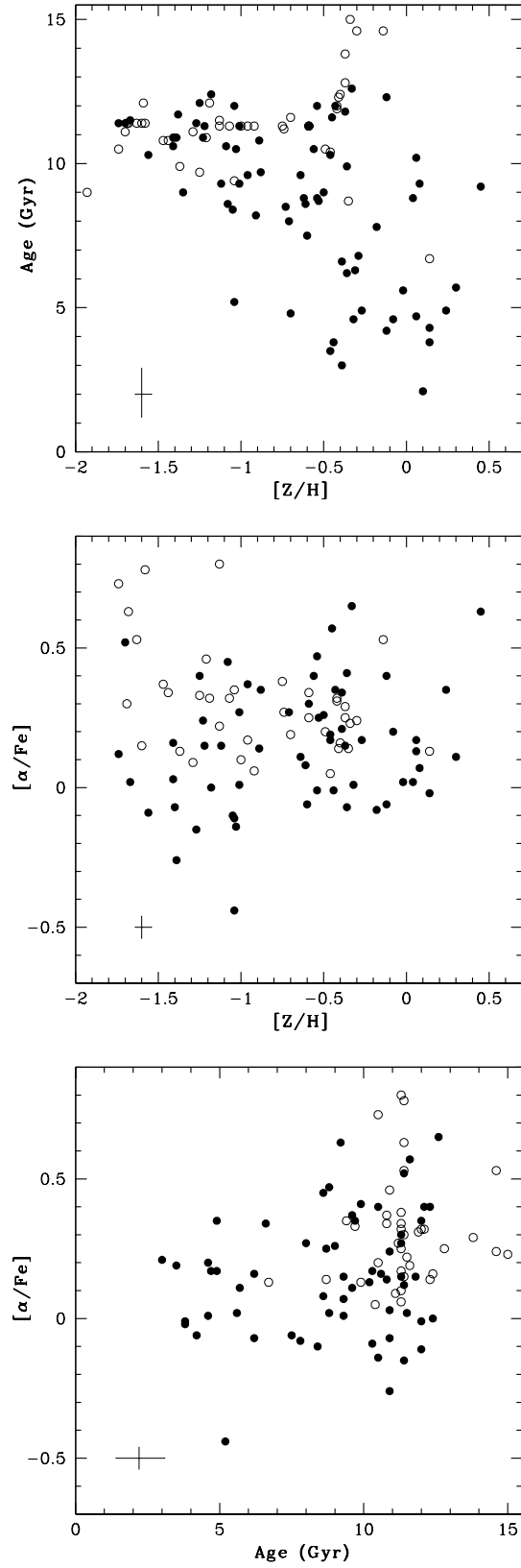


FIG. 13.— Metallicity as a function of age (*top*) and α -to-Fe abundance ratio (*middle*), and age as a function of α -to-Fe abundance ratio (*bottom*) obtained from the SSP models of Thomas et al. (2003) with varying α -elemental abundance (Thomas et al. 2004). The 72 GCs in NGC 5128 are *solid circles* and the 41 Milky Way GCs are *open circles*. The mean uncertainties are displayed in the lower left of each plot.

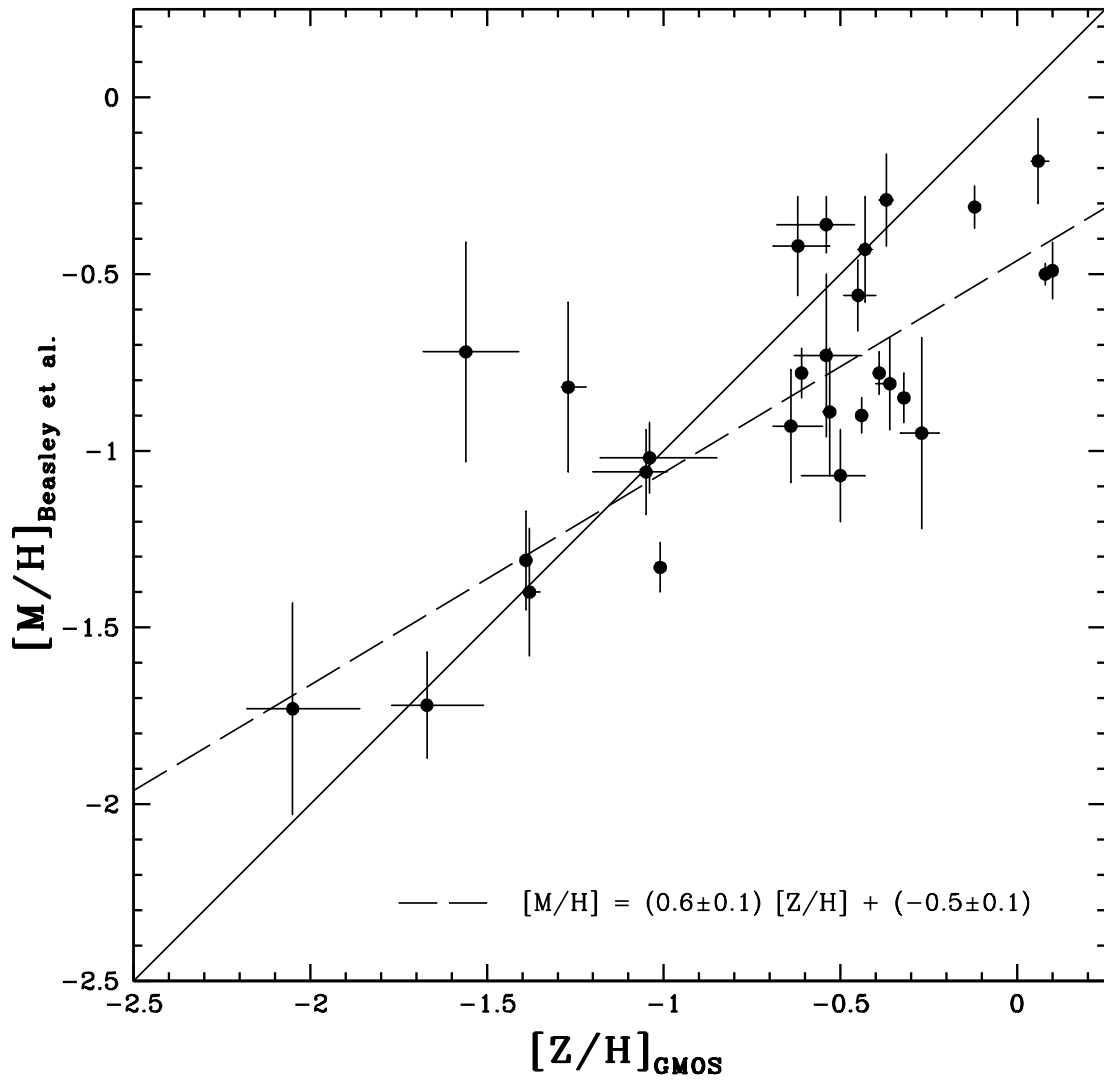


FIG. 14.— Metallicity, $[Z/H]$ derived from the SSP models, compared to empirically derived metallicities of GCs from Beasley et al. (2008). The 1:1 line is shown as a *solid line*. The best fit line is shown as a *dashed line* with a slope and intercept of 0.6 ± 0.1 and -0.5 ± 0.1 and an rms= 0.25.